



Surface Roughness Modeling and Prediction Based on Vibration Signal Analysis and Machining Parameters in Milling of Aluminum by Artificial Neural Network

Sabreen Abdallah Abdelwahab¹

Received: 17 July 2022 / Accepted: 15 January 2023 / Published online: 9 February 2023
© The Institution of Engineers (India) 2023

Abstract For computer numerically controlled (CNC) machines to handle online monitoring and adjustment of machining parameters (MPs) for optimum machining performance, and to achieve high productivity and improve surface quality, online prediction of surface roughness (SR) must be adopted by researchers as an important issue. Studying the MPs' effects on both vibration signal (VS) and SR for aluminum alloy material (AA5083) in a CNC milling machine and developing three models to predict VS and SR based on the artificial neural network (ANN) technique is the aim of this work. The first ANN model was developed to predict vibration frequency and amplitude based on MPs, feed rate “ f ”, depth of cut “ a ”, and cutting speed “ N ”. The second model of ANN was developed to predict SR using MPs as well. The third model of ANN was developed to predict SR using both the MPs and vibration frequency and amplitude. The experiments involved fifteen test specimens. The vibration measurement was performed in the cutting feed direction using the sensor accelerometer that was fixed on the machine tool holder. The readings were recorded online in the MATLAB program, and SR was measured offline. The results showed that the feed rate and depth of cut were the most significant elements that affected the VS, as the VS increased as they increased. The minimum VS and SR values were obtained for the MPs' combinations ($N=23$ m/min, $a=1.5$ mm, and the feed rate values were $f=150, 200,$ and 250 mm/min). The ANN models developed have a feed-forward architecture and supervised learning technique using the algorithm of backpropagation Levenberg–Marquardt and

sigmoid activation function. They are structured into three layers, with the hidden one having eight or ten neurons. The experimental and expected values were very close, and the proposed ANN models have a high correlation factor of $R=0.97-1$ for the prediction of VS and SR values. The third ANN model gave better results in predicting SR. Hence, taking the VS into account improves the capability of the ANN in predicting the SR.

Keywords Vibration signal · ANN model · Surface roughness · Aluminum alloy (AA5083) milling · CNC machine · Sensor accelerometer

Introduction

Manufacturers need automation growth as a method to get higher productivity and improve quality. Computer numerically controlled (CNC) machines have been employed in totally automated machines throughout the earlier eras. Cost, time, and precision are factors considered while selecting a manufacturing process. Dimensional accuracy, surface roughness, and surface performance are often the three factors that determine surface precision [1]. Surface quality contributes significantly to machining performance because a well-machined part's surface enhances corrosion resistance, fatigue strength, creep life [2], strength, and wear [1]. The surface's imperfections, particularly valleys and grooves, create stress concentrations that allow material plastification and cracks to propagate [1].

The surface integrity concept, presented in the literature [3], can be characterized as a collection of different surface-and subsurface-level characteristics of an engineering surface that influence how well the surface performs. Surface roughness, texture, profile, fatigue,

✉ Sabreen Abdallah Abdelwahab
engsabreenabdallah@gmail.com

¹ Production Technology Department, Faculty of Technology and Education, Helwan University, Cairo 11732, Egypt

corrosion, wear resistance, adhesion, and properties of diffusion are a few of these characteristics. Other service characteristics like optical attributes, absorptivity, adsorption, bonding ability, emissivity, flatness, frictional resistance, score strength, stain resistance, surface temperature, surface tension, thermal emissivity, washability, wettability, and biological and chemical properties should be taken into account as well, when appropriate. Geometrical parameters (such as surface finish, texture, and bearing curve parameters), physical parameters (such as micro-hardness, residual stresses, and microstructure), chemical parameters (such as affinity oxidation, adsorption, chemisorption, surface electrical polarization, and surface chemical reactions), and biological parameters are different types of surface integrity parameters (e.g., cell proliferation and cell attachment).

Surface roughness (SR) represents the main property of surface integrity. SR influences numerous practical features, for example, the friction of surfaces induced by contact, wear, light reflection, heat transfer, a lubricant's capability to be distributed and held, fatigue resistance, or coating. Henceforth, the targeted surface finish is stated and a suitable processes are nominated to get the desired quality [2].

Numerous issues may influence the SR in a CNC milling operation. The SR is the sum of the ideal SR resulting from the geometry of the tool and feed rate (FR) “ f ”, and the natural SR resulting from the abnormalities in the cutting process [4]. Additional factors that can affect SR are the machining parameters (MPs) (depth of cut (DC) “ a ”, FR, cutting speed (CS) “ N ”, cooling fluid, process kinematics, step over, and tool angle), cutting tool properties (tool material, tool shape, nose radius, and run out), work piece properties (diameter, length, and hardness), and cutting phenomena (friction, acceleration, chip formation, and cutting force variation) [5]. CS, FR, and DC can be tuned beforehand, while the tool and properties of the workpiece material are unadjustable [6]. SR prediction methods should be developed for products before milling to estimate the suitability of the MPs for achieving the required SR and increasing the quality of the product. These prediction techniques should be reliable, accurate, non-destructive, and low-cost.

The texture of a surface is the outline of the surface that diverges from a nominal reference. The divergence could be recurring or unintended, and it could be brought on by defects, roughness, and waviness [5]. So, the sum of waviness, roughness, and fault form represents the true surface shape. A well-known definition of SR is a sparse, irregular deviation on a scale under waviness. Figure 1 shows the standard terms and symbols for the SR [7]. In machining, SR is usually stated mathematically using the average deviation from the mean:

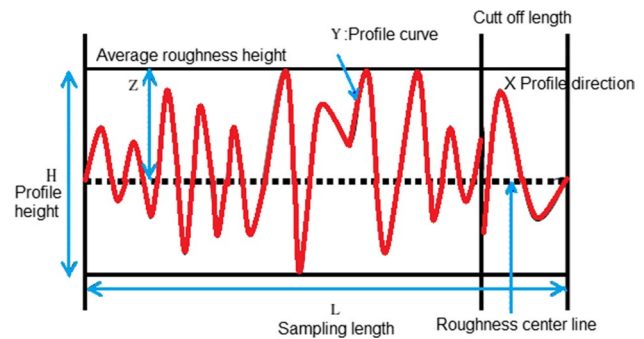


Fig. 1 SR definition terminology, reproduced from [7]

$$Ra = \frac{1}{L} \int_0^L |Y(x)| dx, \quad (1)$$

where L is the sampling interval and Y is the profile curvature's coordinate, and Ra is the sum of the absolute contour height over the evaluation length, or the region in between the roughness contour and its mean line in 1 m, which needs to be optimized [5, 8].

Regarding SR measurement technologies, there are four types of measurement techniques to assess surface geometry and texture: scanning probe microscopy, electronic-type measurement, optical-type measurement, visual-type measurement, and tactile-type measurement. They are reviewed in [3], which provides further details.

Statistical methods and soft computing techniques were used in the modeling and optimization of machining processes. More specifically, the factorial design method, the Taguchi method, response surface methodology, analysis of variance, grey relational analysis, statistical regression methods, artificial neural networks (ANN), fuzzy logic, genetic algorithms (GA), ant colony optimization, expert systems, particle swarm optimization, simulated annealing, various swarm intelligence, adaptive neuro-fuzzy inference systems, and Bayesian networks, which are reviewed for the improvement of machining processes, where these methods have proven to be very powerful and reliable tools, especially in machining [9]. Intelligent machining was also introduced in [1], as various computational techniques are described, such as ANN, fuzzy set theory, and neuro-fuzzy modeling. Moreover, various modeling techniques using the combination of fuzzy logic and GA to construct a model of a physical process, including manufacturing processes, were presented in [10].

SR modeling, optimization, and prediction techniques are categorized into three classes: analytical models, investigational models, and models based on artificial intelligence (AI). Analytical and experimental models are established by means of traditional methods such as statistical regression techniques [2, 11], and linear regression models [12–15].

Instead, models based on AI are developed using nontraditional methods such as ANN [16–20], fuzzy logic, GA [21], and hybrid or mixed systems [22–25]. Researches [8, 20] introduce reviews of the several practices and techniques that are being applied for the prediction of SR.

ANN has been used in SR prediction in milling; Tsai et al. 1999 [26] offered a *Ra* surface recognition system for end milling while processing. Many ANN structures were applied. The three MPs (DC, CS, and FR) and the average vibration per revolution were chosen as independent variables to guess the *Ra*. The ANN model showed a good accuracy rate of 96–99% while predicting *Ra* in comparison to the statistical regression model results. Benardos and Vosniakos [27] constructed a feed-forward ANN to predict *Ra* in a CNC milling process. Many features were chosen as inputs: the three MPs, the cutting tool engagement, wear of the machining tool, and machining forces. A (5 by 3 by 1) structured ANN can expect the SR with a mean-squared error of 1.86%. Topal [19] studied the estimation of SR where a feed-forward ANN was used in the milling process with three layers. It was trained using the backpropagation method. The inputs are the three MPs and the step-over ratio. The average predicted error was 0.04. Oktem et al. [23] suggested an ANN model in addition to the GA approach. The error predicted was no more than 0.0534. Colak et al. [13] suggested a gene formula programming technique built on MPs in CNC milling machines, but there was no quantification for error. Azlan Mohd Zain et al. [28] presented an ANN model for SR prediction in the milling operation. The toolbox of ANN in MATLAB is utilized. Feed-forward backpropagation is the algorithm selected by `learnngdx`, `traingdx`, `logsigm`, and `MSE`, which are the learning, training, transfer functions, and performance, respectively. The (3 by 1 by 1) network structure gave the best ANN model for predicting the SR value. The layers' and nodes' numbers in the layers of the ANN structure could be modified on behalf of improvement. They suggested high CS with a low FR and radial rake angle to get the best SR. Patel et al. [29] decreased the SR through optimizing the numerous MPs of the milling operation. ANN has been implemented. SR was influenced by FR, then CS, and finally DC. Chen et al. [30], a backpropagation ANN was suggested to predict the SR of the workpiece. An analysis of variance was used to investigate the effects of the three MPs and milling length. The mean square error gained through using the backpropagation ANN is much smaller than that gained via the conventional linear regression technique.

Various neuro-fuzzy inference systems (FISs) have also been applied to get the SR in machining processes. The structure of the if–then rules was extracted via the obtainable in–out data. With knowledge of fuzzy rules' number and structure, ANN and GA's optimization methods are applied to modify the shape of the membership function of the fuzzy

variables and the parameters of the fuzzy rule base. Lo [24] considered the application of an adaptive FISs (ANFIS) to forecast the workpiece SR afterward the milling operation. Two dissimilar membership functions, trapezoidal and triangular, were assumed throughout the training operation of ANFISs to correlate the accurateness of SR prediction by both networks. The triangular membership function gave a higher accuracy in prediction. Abdel Badie Sharkawy [31] presented an end milling process SR model. Several intelligent networks have been used: radial basis functions neural networks (RBFNs), ANFISs, and genetic FIS. The three MPs have been utilized as inputs to model the SR with the highest accuracy. Experimental data was used to train the networks. It is determined that ANFIS has a local minima issue, and perfect optimality cannot be insured by Genetic FISs unless using appropriate parameters such as (number of generations, population size, etc.). The RBFN model gave the best performance. Vallejo et al. [32] established an online SR forecast module for peripheral end milling. An ANN model using five MPs and one variable signal was developed. High correlations with the SR in the workpiece were shown by the vibration signal (VS). Wu and Lei [5] examined the possibility of using the VS features measured and the MPs in the milling operation to predict the SR of S45C steel. The VS's features are taken out by the envelope investigation and statistical calculation, as kurtosis, root mean square, multi-scale entropy, skewness, and frequency normalization. The MPs' and the VS's features were used to improve the accuracy of SR prediction through the milling operation.

Built on the preceding studies [33–40], the capabilities of ANN for machining process modeling can address the next issues: ANN can deal with nonlinear modeling where the input data is mapped to the output data. Compared to conventional techniques, ANN has advantages such as speed, simplicity, and a high capacity for learning from available data sets. It does not need much experimental data, and no initial assumptions are needed. Experimental results' behavior can be improved easily and in a small duration. The performance of the ANN prediction model can be enhanced by using trial-and-error approaches and frequent training simulations. Further, ANN has some limitations in machining operation modeling, such as experimental practices are essential in building a realistic network. It may be time-consuming and cost a lot. Training repeatability for an enhanced model is not certain. Using the ANN, the greatest prediction model for SR can be reached by using a trial-and-error technique with adjusting the ANN model structure. Furthermore, the workpiece's SR is attributed to both the MPs' effect and the machine vibrations' effect in the milling operation.

Gaining a good surface finish is a vital issue in every engineering part's design and manufacturing. Consequently, measurement, characterization, and prediction of SR play an important role in the assignment of machining performance.

This work focuses on an experimental study of the effect of MPs on VS and SR results in the aluminum alloy AA5083 end milling process and developing three ANN models for potential use in the online prediction of VS and SR in a CNC milling machine. The first model will be developed to predict the VS amplitude and frequency related to the selected MPs set. Another ANN model will be developed to predict the average SR value against the selected MPs values. The last ANN model will be developed to predict the average SR value against the combination of the selected MPs set and the VS amplitude and frequency. These ANN models will represent an experimental guide for workers to select optimum MPs of aluminum alloy AA5083 milling that guarantee an optimum material removal rate without unwanted vibrations and with a good surface finish. Milling experiments are accomplished with different sets of machining conditions: CS, FR, DC, and with the use of a coolant. The results will be utilized in inferring the relationship between the selected machining conditions and the measured VS and SR during the milling process.

Artificial Neural Network Modeling Technique

AI techniques such as ANN and fuzzy logic have been widely used in the development of predictive models [41, 42]. ANNs are widely utilized in a variety of fields, containing mathematics, economics, engineering, and medicine. For different purposes, ANNs are used in data compression, optimization, forecasting, pattern and voice recognition, classification, and vision systems. Currently, ANNs are capable of recognizing sophisticated problems that present a challenge to the old-style techniques [43, 44]. ANNs have been considered to resolve issues concerning missing or inaccurate data [45]. The benefits of ANNs are flexibility, speed, and the ability to learn from examples as compared to classical methods. Hence, engineering work in these fields can be decreased. ANNs can deal with nonlinear problems and show robustness and fault tolerance, but they cannot deal with problems demanding great precision and exactness, as in arithmetic and logic problems [44].

The ANN methodology simply allows a computer to simulate human brain neurons' attitudes. It is commonly structured into layers; each layer comprises a number of neurons. An ANN is trained by employing a set of input and output data. During training, the model's structure automatically adapts to the data, and the resulting model can be used to make predictions. The training method is clearly described as a process that involves controlling a network's weights and biases in order to reduce the error of the chosen function between the desired and actual outputs [46]. Backpropagation is the most

widely used and extensively researched supervised learning training algorithm. The mean-squared error of the difference between the network outputs and the targets in the training set is minimized using a gradient-descent approach [45]. The basic steps for network training are completed by doing the following actions: calculations of the related output value using the ANN after applying the input data. Find the incorrect value by comparing the output to the desired result. To change each weight for error reduction, consider the changes and the orientation (positive or negative) of the weights. Determine the new weights' values. Apply the weight modifications. With each training input–output data set, repeat the previous stages until the error is at a desirable level. The output of the layers is passed through activation functions by the ANNs. These activation processes scale the ANN's output into the appropriate ranges. The sigmoid function used for activation is the standard option for the feed-forward layer:

$$f(x)_1 = \frac{1}{1 + e^{-x}}, \quad (2)$$

where x is the input value.

The classic neuron is composed of a linear activator and a nonlinear constraining function. The linear activator function of the classic neuron produces the sums of the weighted inputs together with an additional independent term known as bias [47].

The hidden layer employs a sigmoid-type transference function:

$$f(x)_2 = \frac{1}{1 + e^{(-b - \sum w_i x_i)}}, \quad (3)$$

The last layer (output layer) utilizes a linear function:

$$\text{Output} = \left(\sum_{i=0}^{n-1} w_i x_i \right) + b_n, \quad (4)$$

where x_i is the input value number i , n the total number of input–output data sets, w the weight value, i the number of input–output data set, and b the bias value.

Experimental Work

Experimental Setup

Aluminum alloy (AA 5083) material has been selected for the end milling operations. Tables 1 and 2 contain specific information on the AA 5083 alloy's chemical content and mechanical characteristics. The CNC milling machine used for the investigation is the Intelys C3000 CNC milling machine, a three-axis, high-speed machine. Machine mechanical and physical properties are attached

Table 1 AA5083 alloy’s chemical composition [48]

Mn	Fe	Cu	Mg	Si	Zn	Cr	Ti	Al
0.40–1	0.40	0.10	4–4.90	0.40	0.25	0.05–0.25	0.15	Balance

Table 2 Mechanical properties of the AA5083 alloy [48]

Hardness Vickers	Shear strength	Elongation	Tensile strength	Proof stress
75 HV	175 MPa	23%	300 MPa	145 MPa

Table 3 Intelys C3000 physical and mechanical properties

Property	Value
Max chuck speed (r/min)	3000
Min chuck speed (r/min)	100
Processor frequency (Hz)	2,000,000
Max FR (mm/min)	700

in Table 3. In Fig. 2, the experimental setup is displayed. The machining operations were performed using a high-speed steel end mill tool with a parallel shank, 4 flutes, a 6 mm diameter, and a 40 mm length. An emulsified coolant was used.

Vibration Measurement and Analysis Techniques

An accelerometer sensor was used in measuring the VS. The accelerometer model is (333B32 Model Array), a ceramic shear ICP[®] accelerometer with 100 mV/g, 0.5–3 kHz, and a 10–32 side connector. Its operation is based on the deformation of the sensing element, which results from the internal force of the mass element due to its acceleration. This deformation change leads to a change in the resistance of the element and hence the electric output of the accelerometer. The

accelerometer was fixed to the tool holder. It was calibrated by employing a double-ended reference (comparison) accelerometer, which is a convenient way to conclude the sensitivity and frequency response characteristics of indefinite displacement, velocity, and acceleration sensors. A vibration laboratory equipped with an electrodynamic shaker and control system that can simply employ the reference accelerometer to achieve in-house calibrations is used. The shaker detrain PCB was used to calibrate the accelerometer.

The data acquisition system used in the experiments was the LMS Pimento instrument system. This was used in data acquisition and signal processing. The accelerometer data was acquired as a time domain acceleration signal (measured raw signal) to be sent to the computer, with the measured signal band width set to 0: 25 kHz and the sampling time set to 0.00002 s. Table 4 summarizes the specifications of the data acquisition system. Measuring raw signals were transformed into the frequency domain using fast Fourier transform (FFT) in MATLAB software, and the vibration amplitude and frequency were assigned. A schematic diagram of the system is displayed in Fig. 3a, and the data acquisition system is shown in Fig. 3b.

Experiments Plan

The MPs proposed in this work to machine AA 5083 aluminum alloy are selected and displayed in Table 5. Then, in order to study the effect of MPs on VS and SR, different combinations of the selected cutting conditions are made to find the effect of each parameter independently.

Five experiments have been performed at different surface CSs to study the CS effect. These are 19, 21, 23, 25, and

Fig. 2 Experimental setup

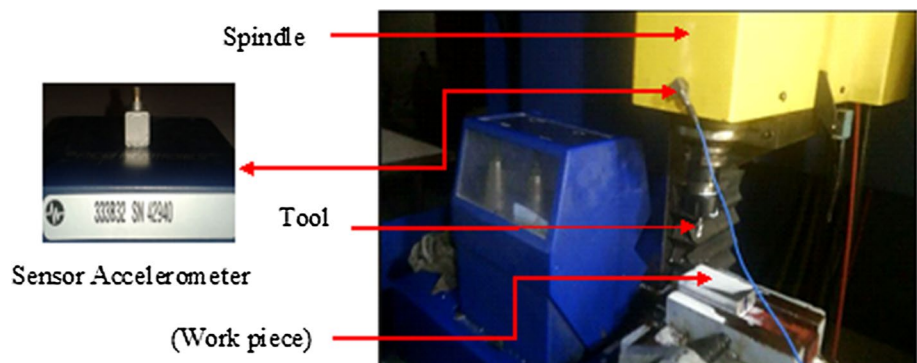


Table 4 Data acquisition system specifications

Property	Value
Model	Asp 424
Number of input channel	4
Number of output channel	1
Interface to computer	IEEE1394A Fire wire
Power	DC power input

Table 5 The selected cutting conditions

Cutting condition	Selected values
CS (m/min) “ N ”	19, 21, 23, 25 and 27
FR (mm/min) “ f ”	150, 200, 250, 300 and 350
DC(mm) “ a ”	0.7, 1, 1.5, 2, and 2.3

Table 6 MPs combinations to study CS effect on VS and SR

Experiment no.	Machining parameters' combinations		
	N (m/min)	f (mm/min)	a (mm)
1	19	250	1.5
2	21	250	1.5
3	23	250	1.5
4	25	250	1.5
5	27	250	1.5

27 m/min, whereas keeping the FR and DC values constant at $f=250$ mm/min and $a=1.5$ mm, as shown in Table 6. Moreover, to study the DC effect, an additional five experiments have been performed at different DC values. These are 0.7, 1, 1.5, 2, and 2.3 mm, while keeping the CS and FR values constant at $N=23$ m/min and $f=250$ mm/min, as presented in Table 7. Additionally, in order to study the FR influence, another five experiments have been performed at different FR values. These are 150, 200, 250, 300, and 350 mm/min while keeping the CS and DC values constant at $N=23$ m/min and $a=1.5$ mm, as shown in Table 8.

Table 7 MPs combinations to study DC effect on VS and SR

Experiment no.	Machining parameters' combinations		
	N (m/min)	f (mm/min)	a (mm)
6	23	250	0.7
7	23	250	1
8	23	250	1.5
9	23	250	2
10	23	250	2.3

Table 8 MPs combinations to study FR effect on VS and SR

Experiment no.	Machining parameters' combinations		
	N (m/min)	f (mm/min)	a (mm)
11	23	150	1.5
12	23	200	1.5
13	23	250	1.5
14	23	300	1.5
15	23	350	1.5

Fifteen test specimens were prepared with $60 \times 40 \times 15$ mm dimensions. A total of 125,000 reads per sample were taken at each experiment for 25 s through 5 reading sections, where each reading section duration was 5 s. The recorded VSs during milling were analyzed and studied in the frequency domain.

After the measurement of the VS for all test samples, the SR (R_a ; the surface roughness arithmetic mean) of each sample was measured offline by a mobile roughness measurement device (model: Mitutoyo SJ-210) as shown in Fig. 4. Three SR values, R_a , were taken for each sample at different places. Then the average SR value was calculated.

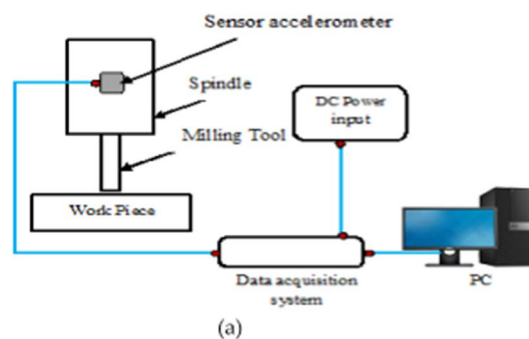
Fig. 3 a Schematic diagram of the experimental setup system, and b Data acquisition system



Fig. 4 Surface roughness measurement device

Results

With respect to MPs’ effects on VS and SR values, Figs. 5, 6, 7, 8, 9, 10, 11, 12, 13, 14, 15, 16, 17, 18 and 19 show the time-domain VSs in the cutting feed direction (raw signal), and the signal frequency analysis in the frequency domain for different MPs’ combinations. The highest vibration amplitudes in the cutting feed direction and their related frequency values were assigned for interpretation. Table 9 shows the average SR values related to different MPs’ combinations in each experiment. And Table 10 illustrates the

maximum six values of amplitude in both frequency and time domains and their related time and frequency values for the 15 experiments. X is the time, and Y is the amplitude in the time domain. $X1$ and $Y1$ are the frequency and amplitude values in the frequency domain. Adding to that, Figs. 20, 21, 22, 23, 24 and 25 show the relationship between the VS amplitude and frequency and the different MPs’ combinations, while Figs. 26, 27 and 28 show the relationship between the SR and the different MPs’ combinations.

Considering the CS effect, Figs. 5, 6, 7, 8 and 9 express the CS effect on VS. The highest signal amplitude values ranged from 3200 decibels (dB) to 28,570 dB, and the related frequency values were 50, 100, 200, and 300 Hz. The highest amplitude values were observed at frequencies of 50 and 100 Hz. Excluding these frequency values, steady machining was achieved throughout the frequency range up to 25,000 Hz. The maximum amplitude value in the time domain was 14.5 mm/s^2 for experiment 5 ($N=27 \text{ m/min}$, $f=250 \text{ mm/min}$, $a=1.5 \text{ mm}$). Figures 20 and 21 illustrate the relationship between VS amplitude and frequency and the CS. In Fig. 20, the highest amplitude value is at $N=27 \text{ m/min}$, and the lowest value is at $N=25 \text{ m/min}$, while $N=19$ and 23 m/min gave the mean amplitude values. In Fig. 21, the highest frequency value is at $N=23 \text{ m/min}$ and the lowest value is at $N=25 \text{ m/min}$. Further, the highest SR value was $Ra = 3.068 \text{ }\mu\text{m}$ at $N=19 \text{ m/min}$ and

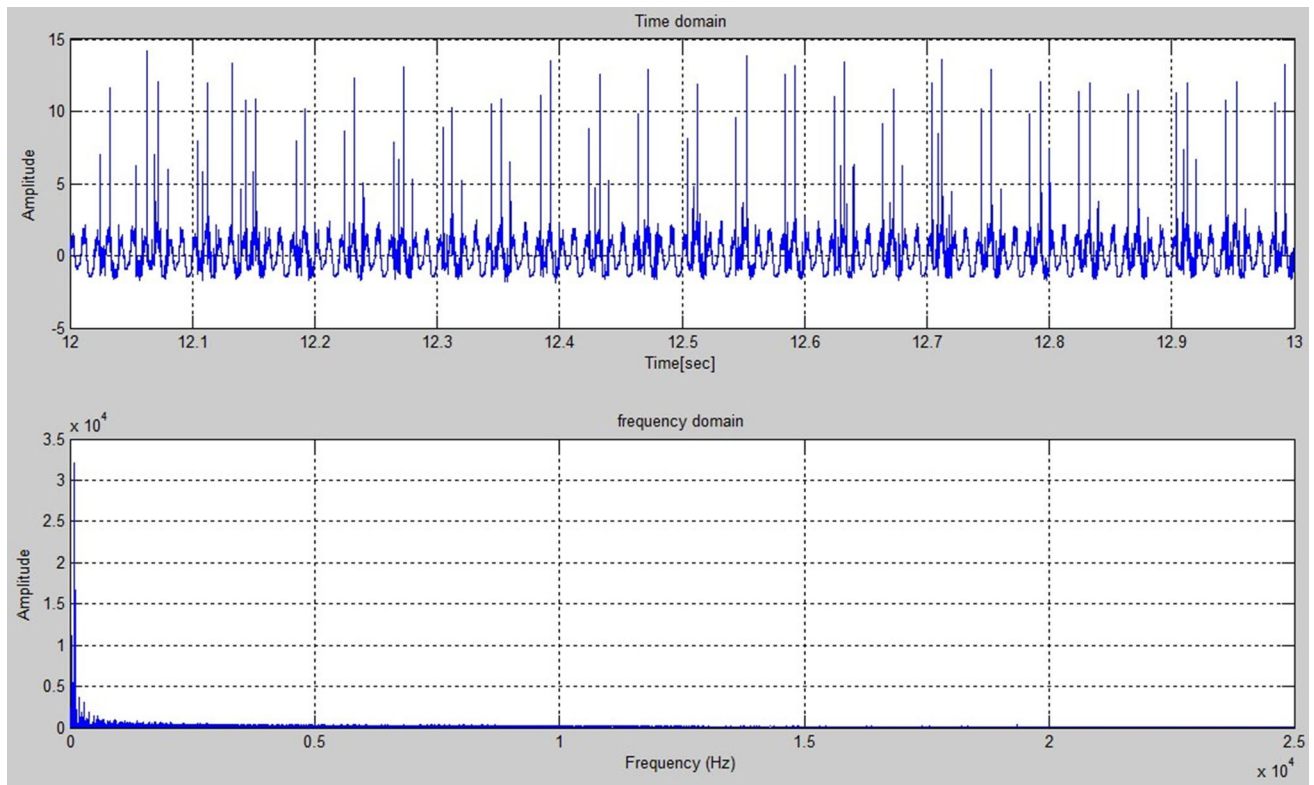


Fig. 5 Raw signal and frequency analysis at ($N=19 \text{ m/min}$, $f=250 \text{ mm/min}$, and $a=1.5 \text{ mm}$), experiment 1

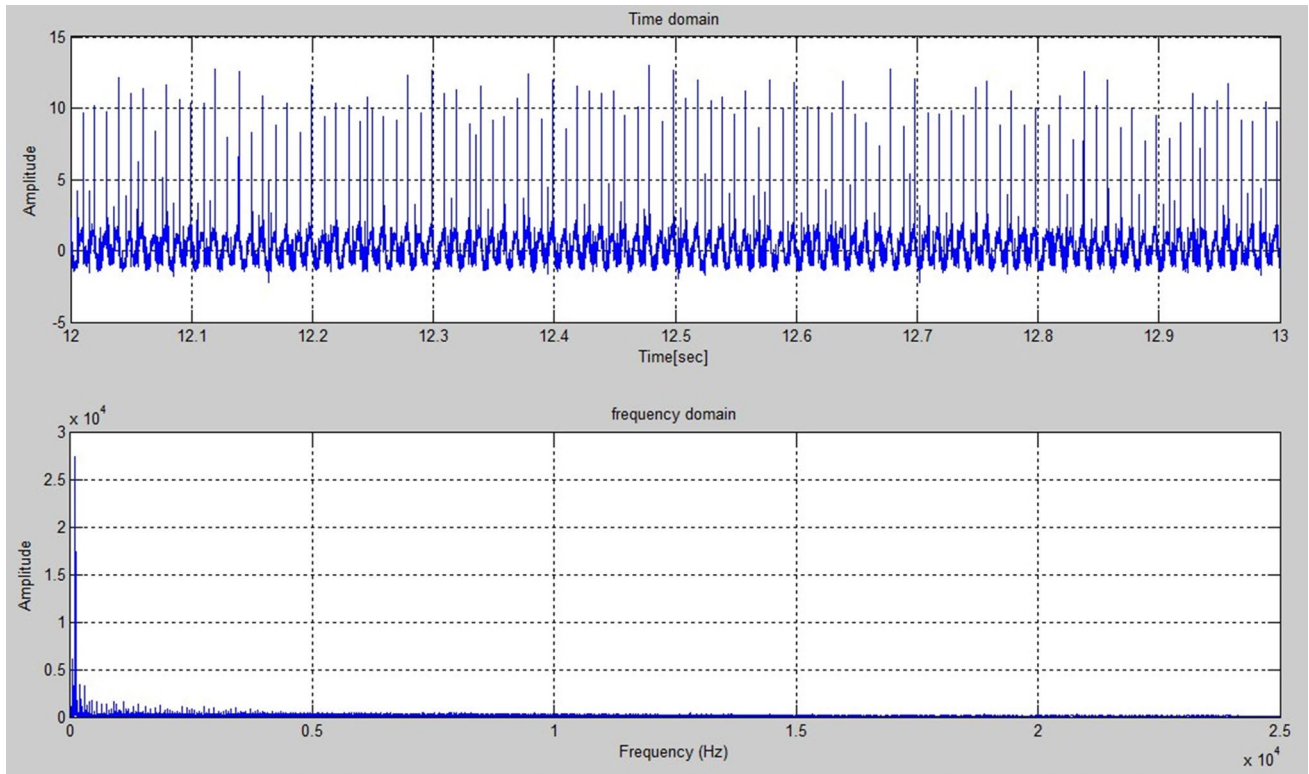


Fig. 6 Raw signal and frequency analysis at $N=21$ m/min, $f=250$ mm/min and $a=1.5$ mm, experiment 2

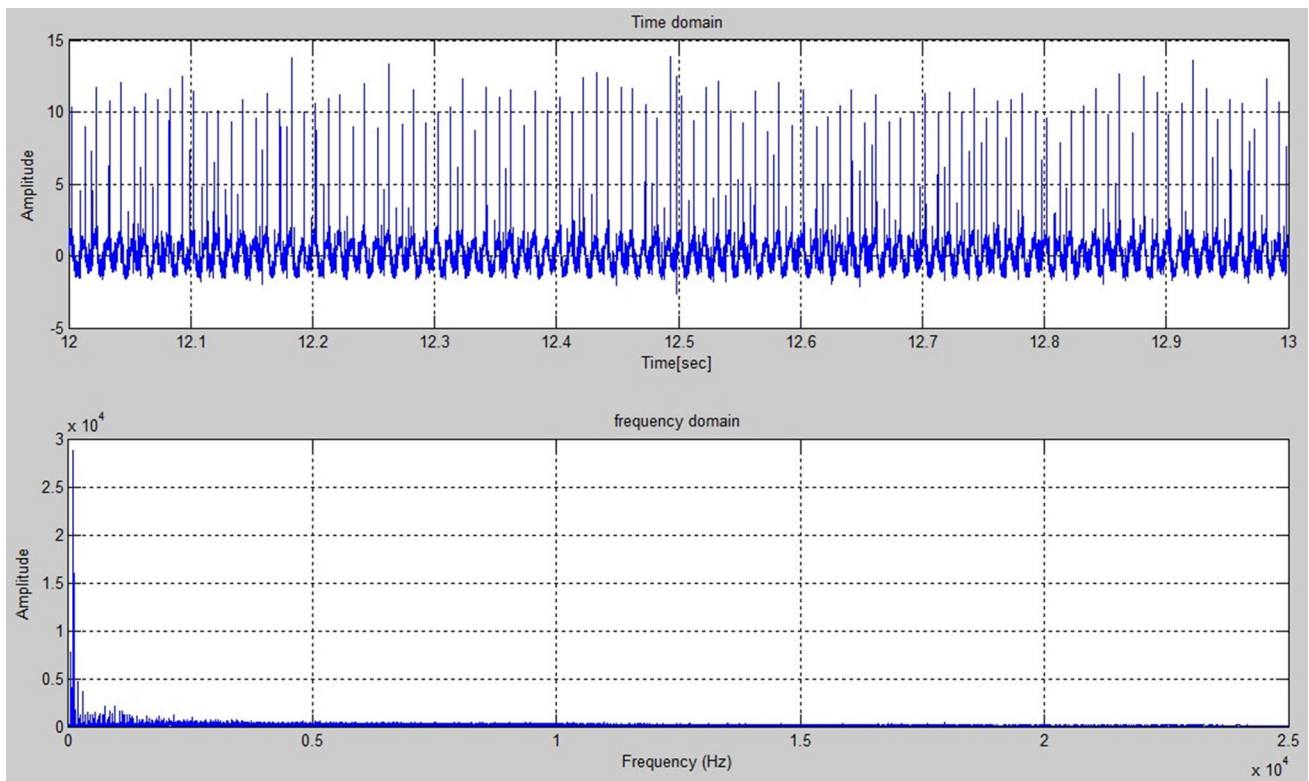


Fig. 7 Raw signal and frequency analysis at $N=23$ m/min, $f=250$ mm/min and $a=1.5$ mm, experiment 3

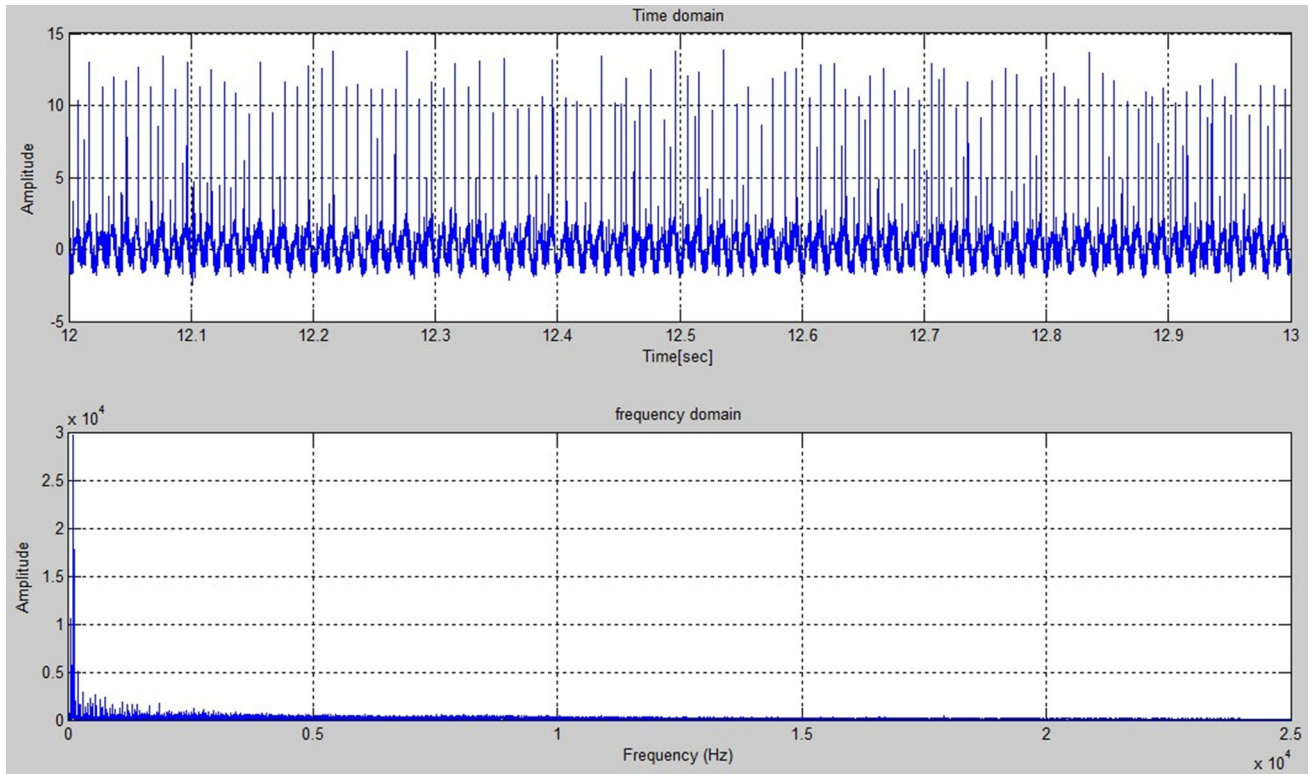


Fig. 8 Raw signal and frequency analysis at $N=25$ m/min, $f=250$ mm/min, and $a=1.5$ mm, experiment 4

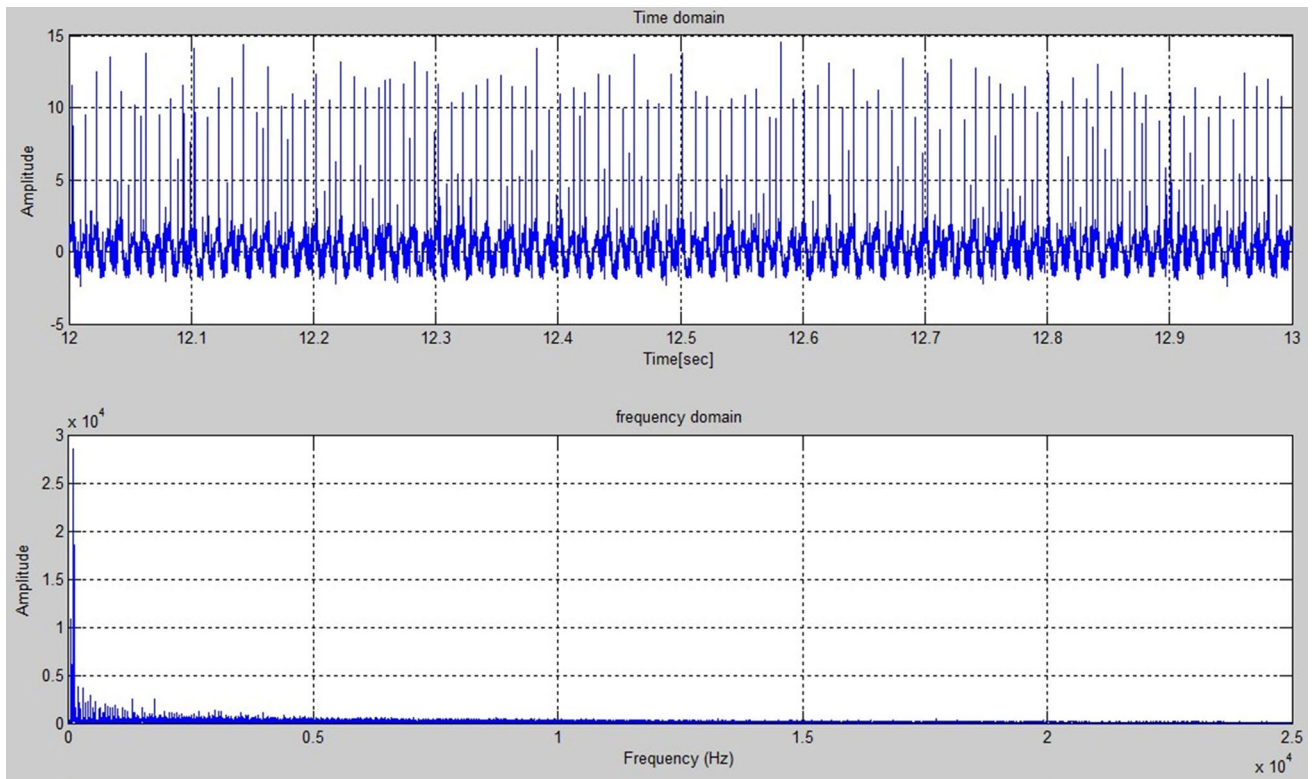


Fig. 9 Raw signal and frequency analysis at $N=27$ m/min, $f=250$ mm/min and $a=1.5$ mm, experiment 5

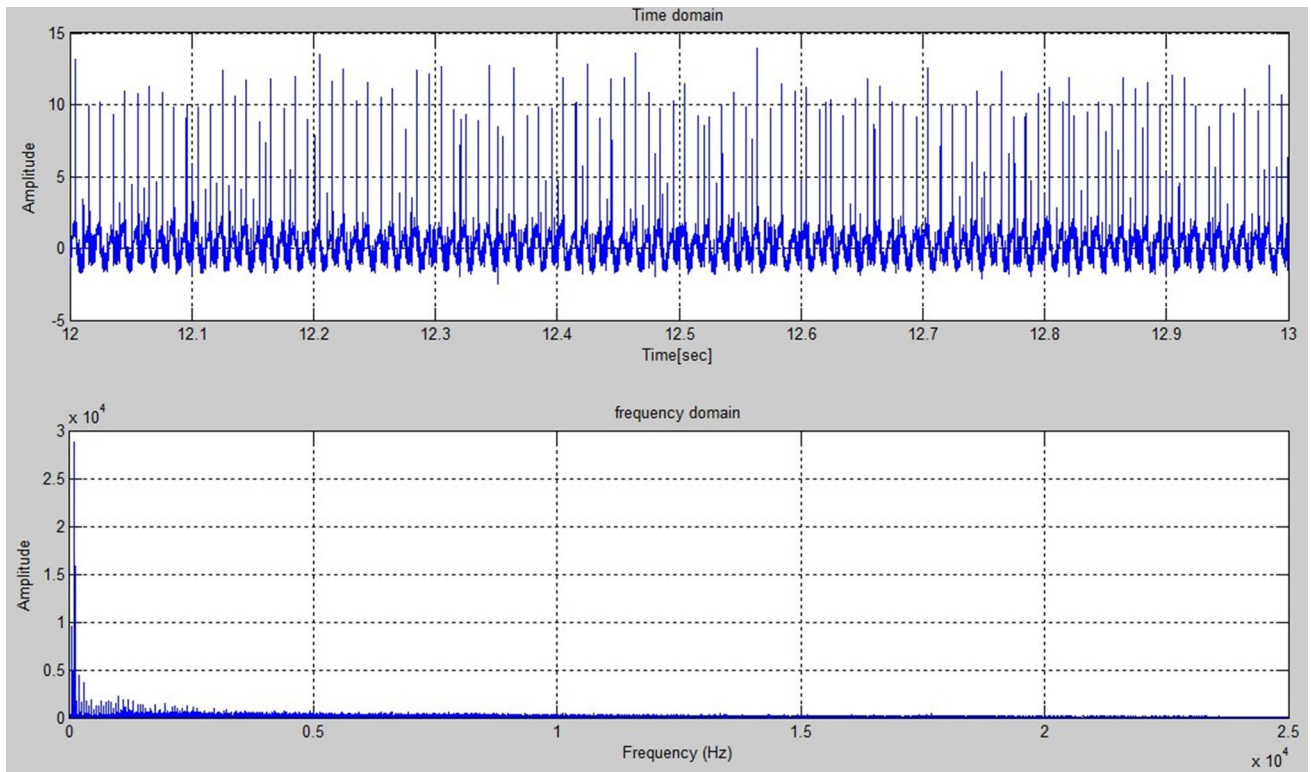


Fig. 10 Raw signal and frequency analysis at $N=23$ m/min, $f=250$ mm/min and $a=0.7$ mm, experiment 6

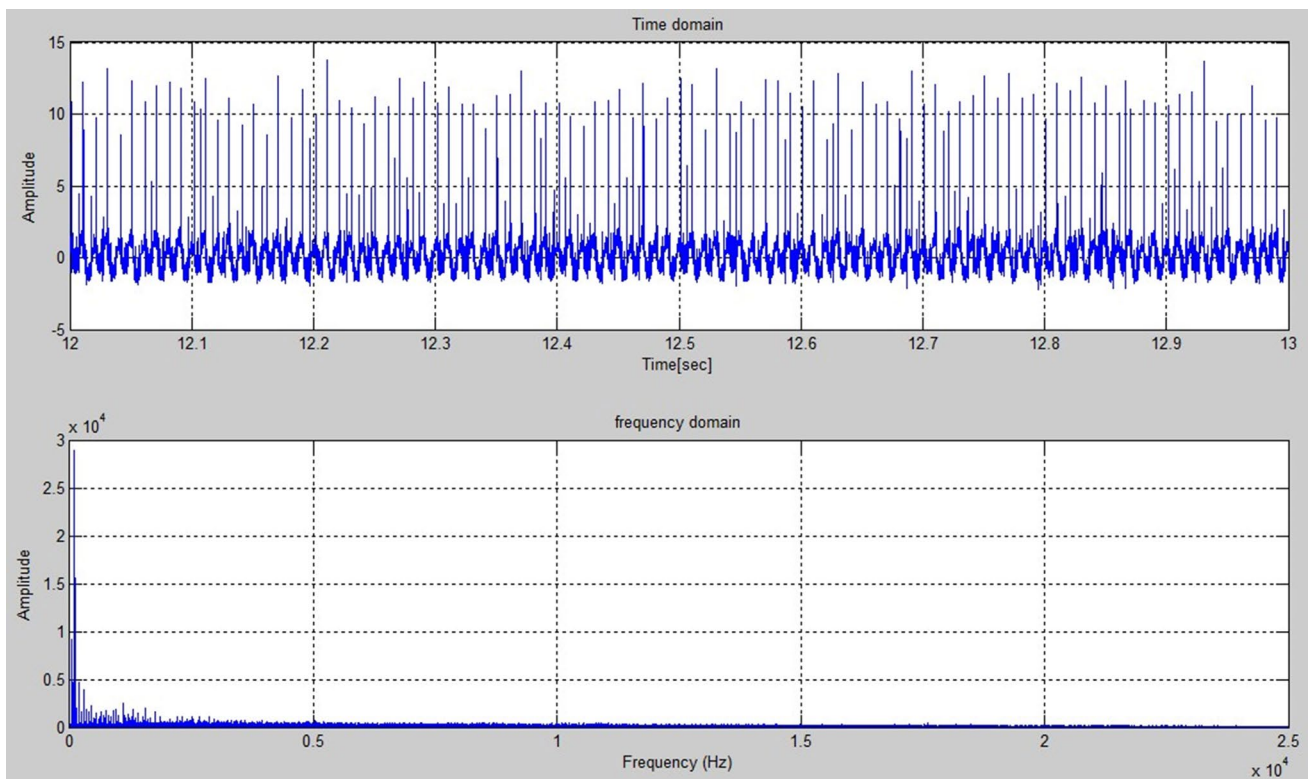


Fig. 11 Raw signal and frequency analysis at $N=23$ m/min, $f=250$ mm/min and $a=1$ mm, experiment 7

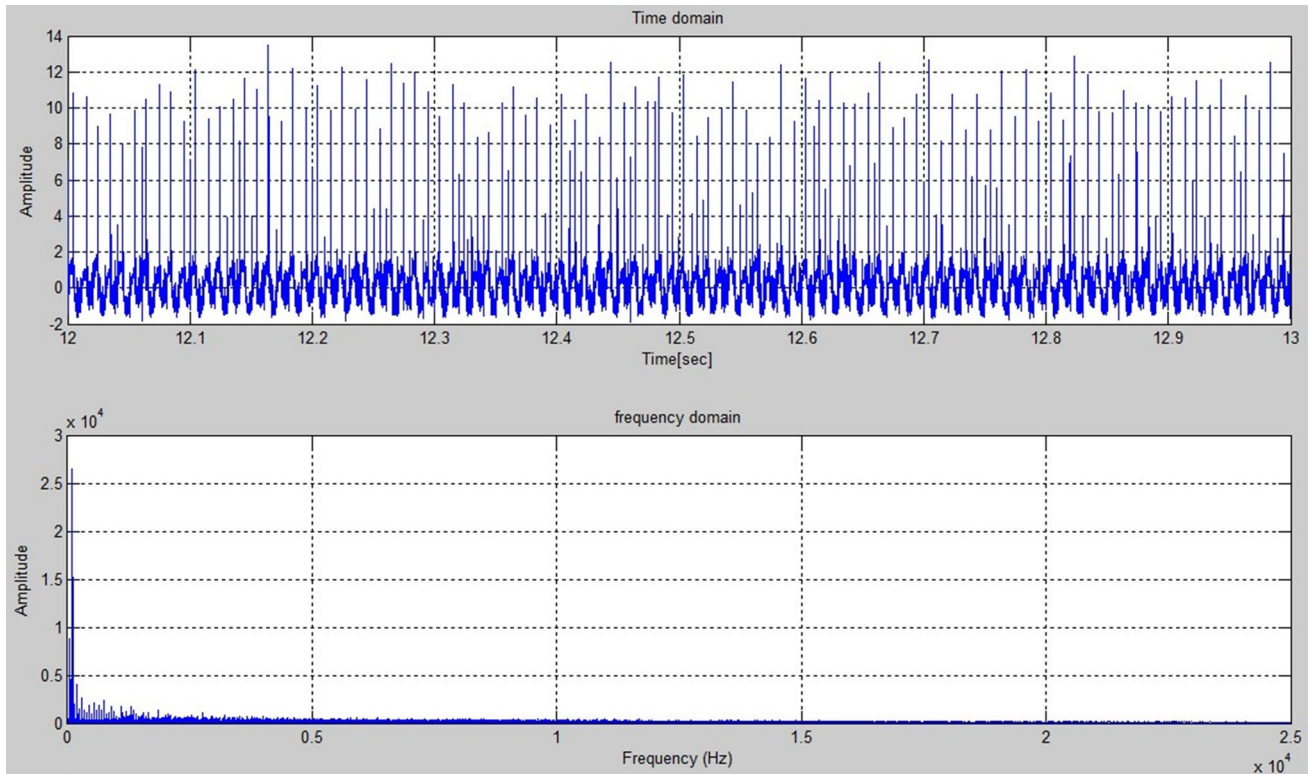


Fig. 12 Raw signal and frequency analysis at $N=23$ m/min, $f=250$ mm/min and $a=1.5$ mm, experiment 8

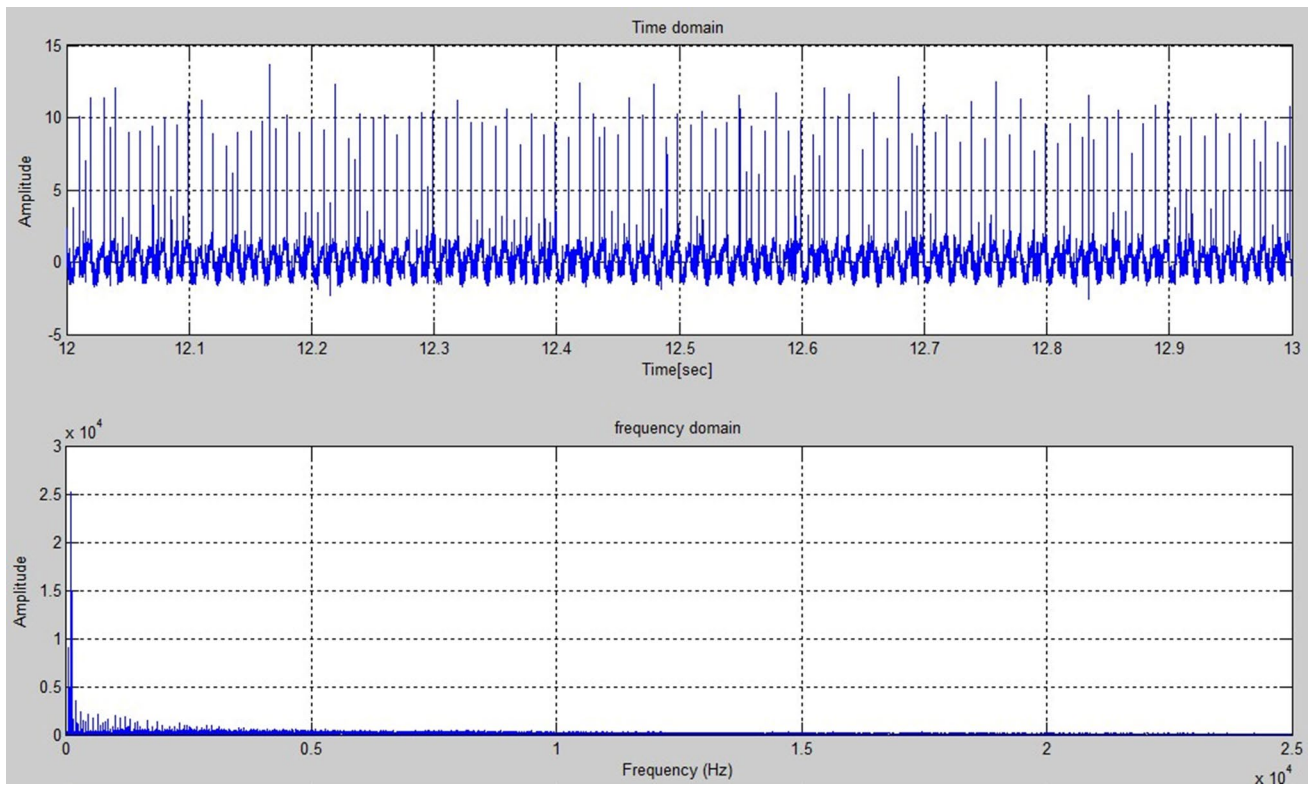


Fig. 13 Raw signal and frequency analysis at $N=23$ m/min, $f=250$ mm/min and $a=2$ mm, experiment 9

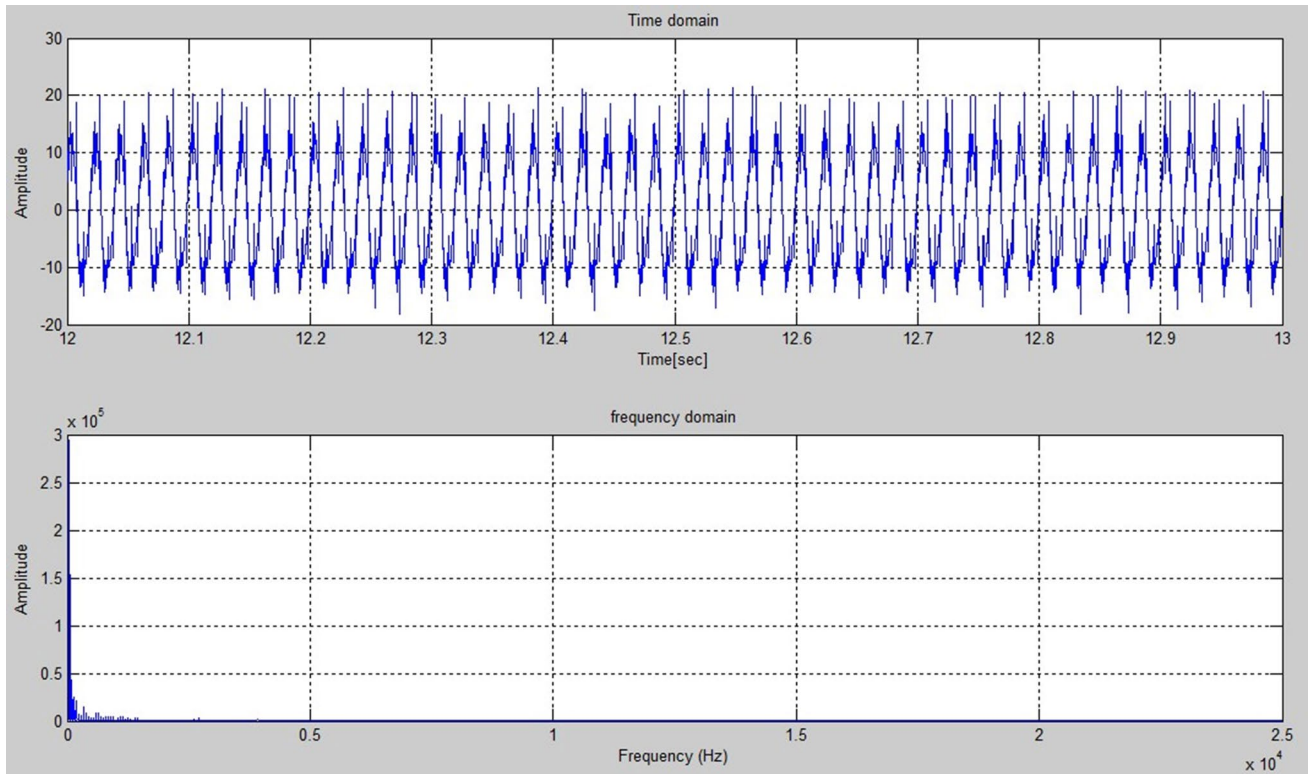


Fig. 14 Raw signal and frequency analysis at $N=23$ m/min, $f=250$ mm/min and $a=2.3$ mm, experiment 10

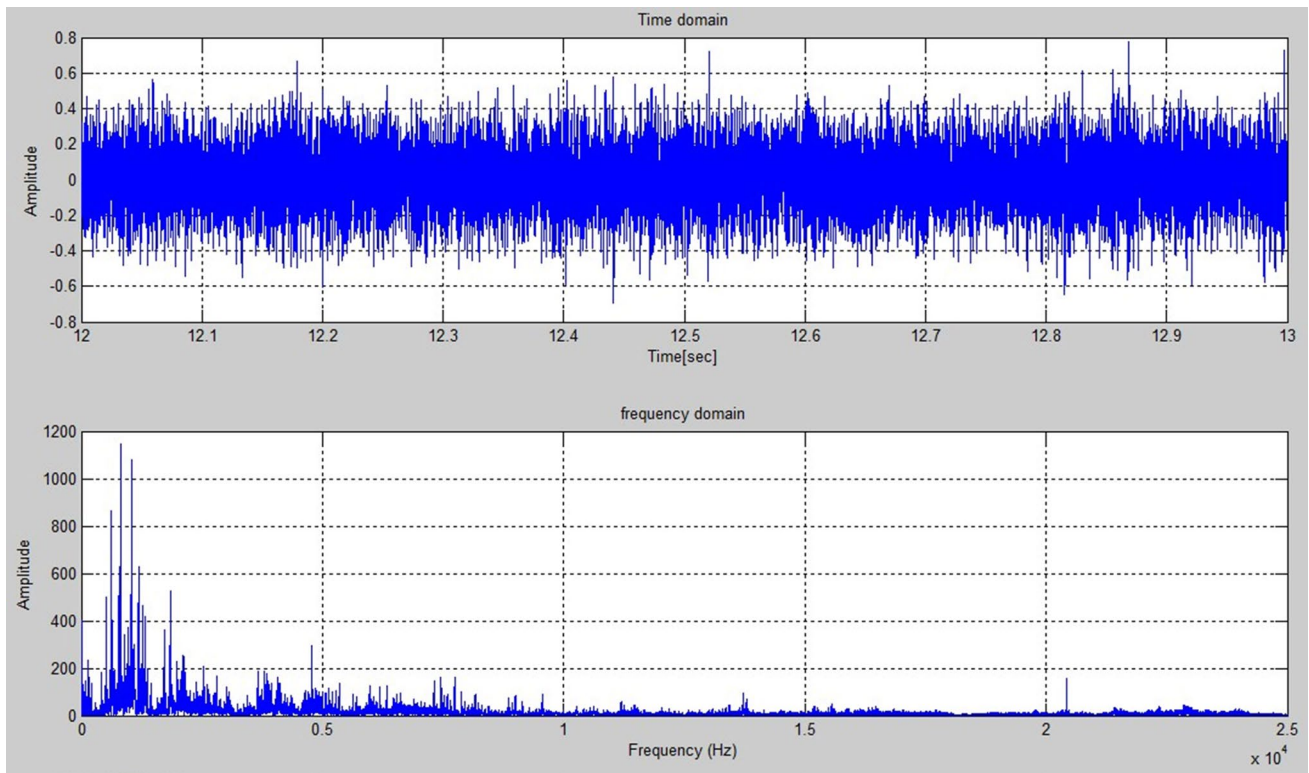


Fig. 15 Raw signal and frequency analysis at $N=23$ m/min, $f=150$ mm/min and $a=1.5$ mm, experiment 11

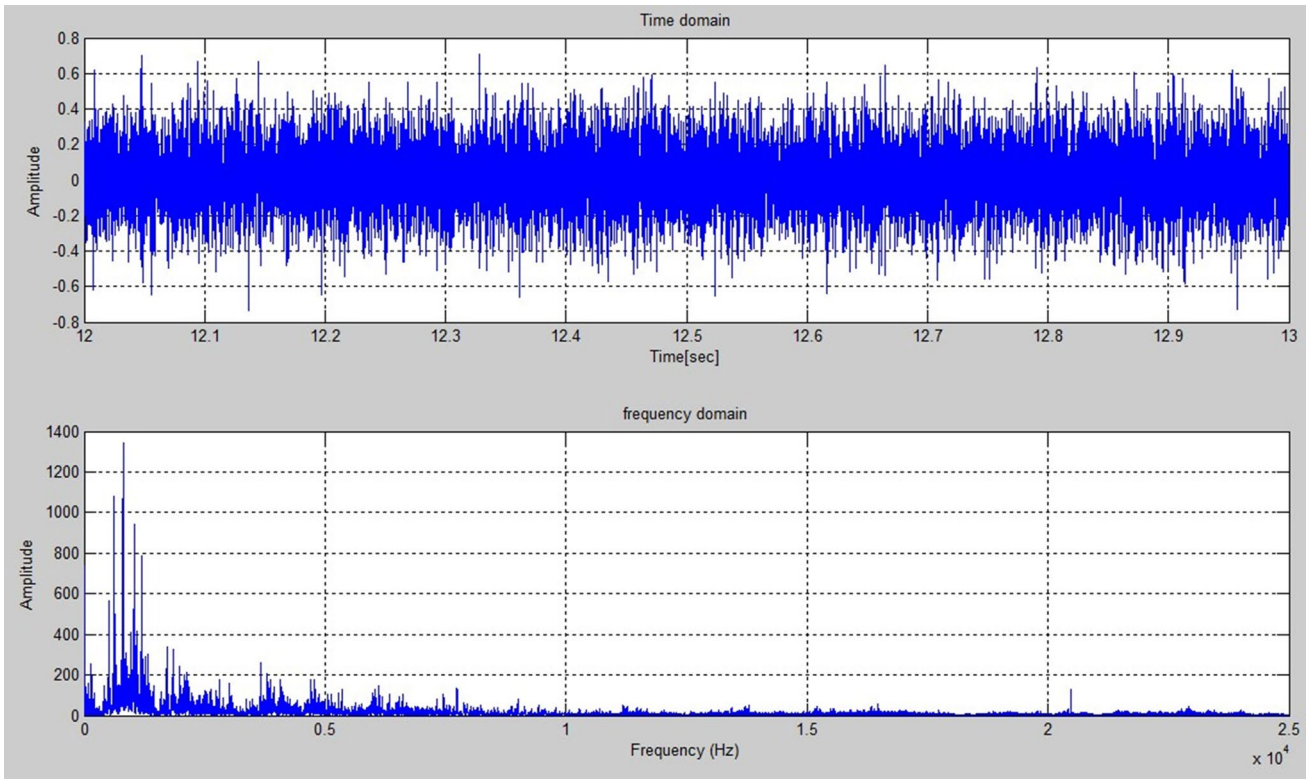


Fig. 16 Raw signal and frequency analysis at $N=23$ m/min, $f=200$ mm/min and $a=1.5$ mm, experiment 12

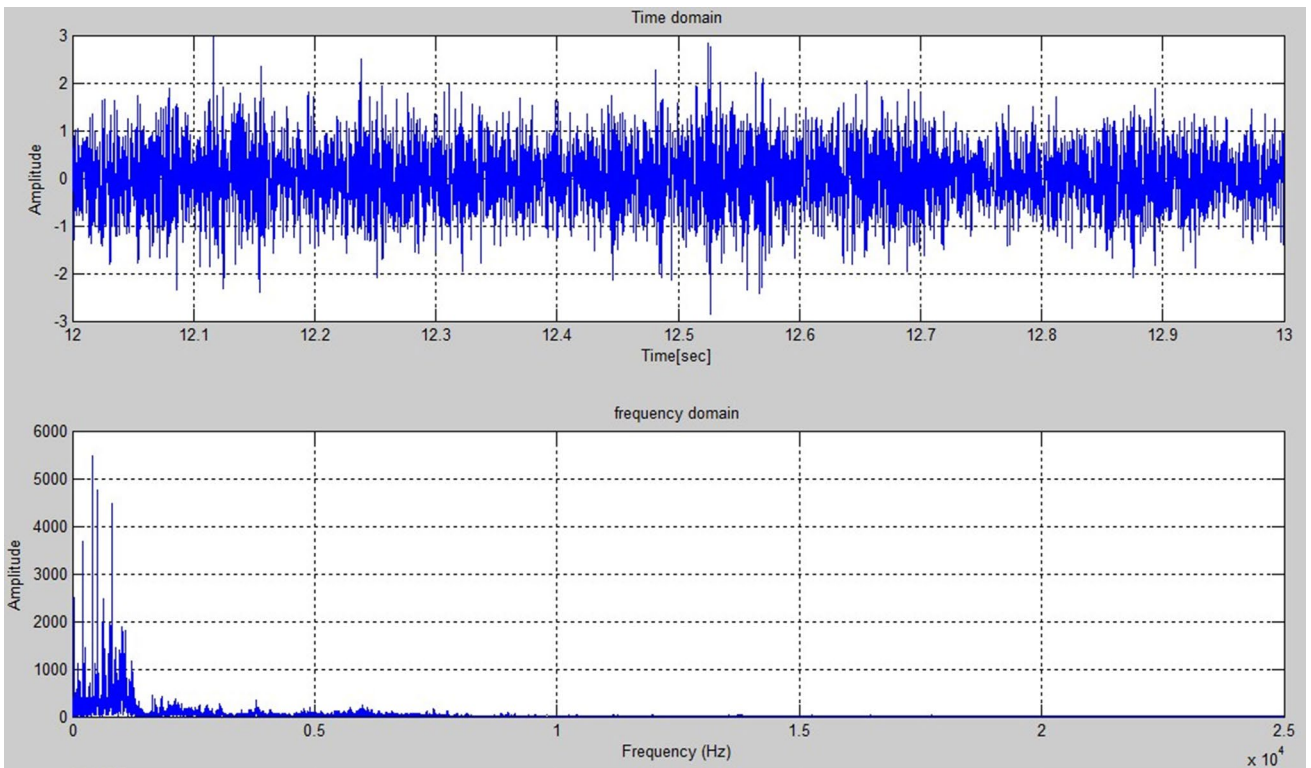


Fig. 17 Raw signal and frequency analysis at $N=23$ m/min, $f=250$ mm/min and $a=1.5$ mm, experiment 13

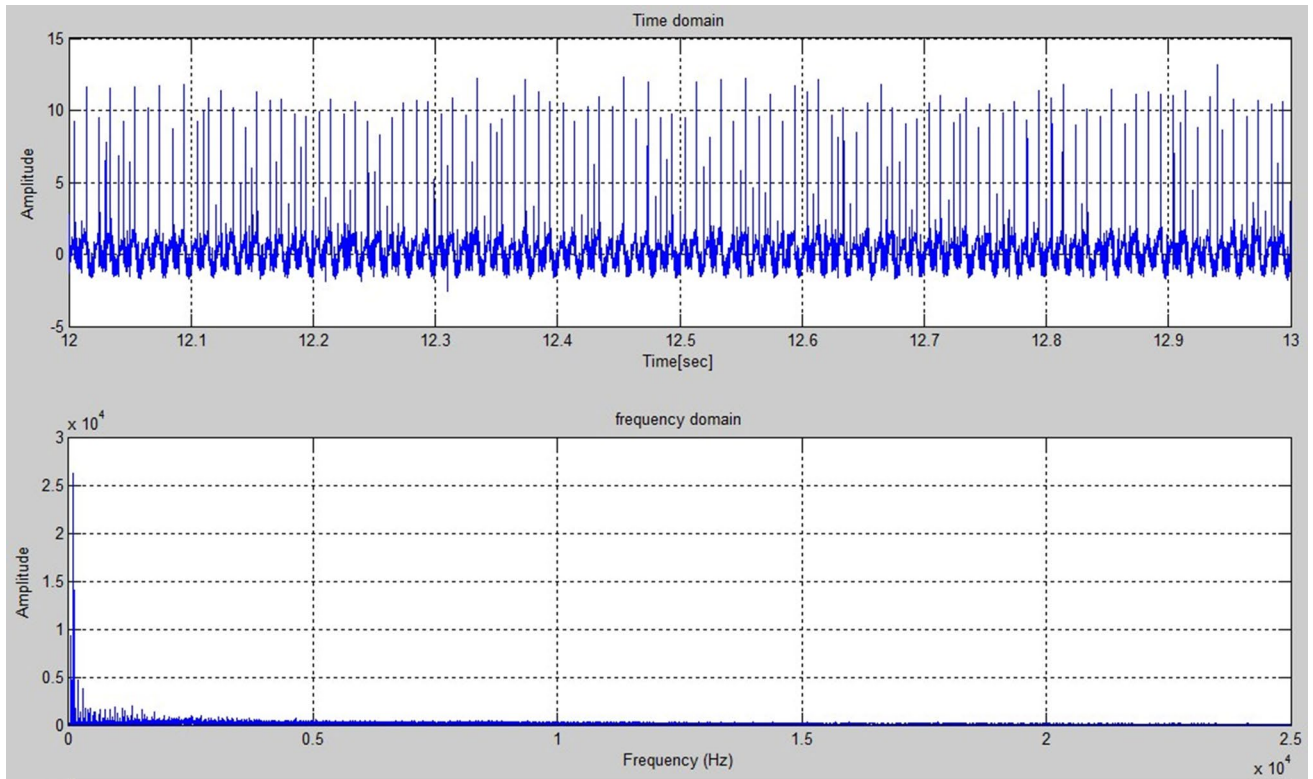


Fig. 18 Raw signal and frequency analysis at $N=23$ m/min, $f=300$ mm/min and $a=1.5$ mm, experiment 14

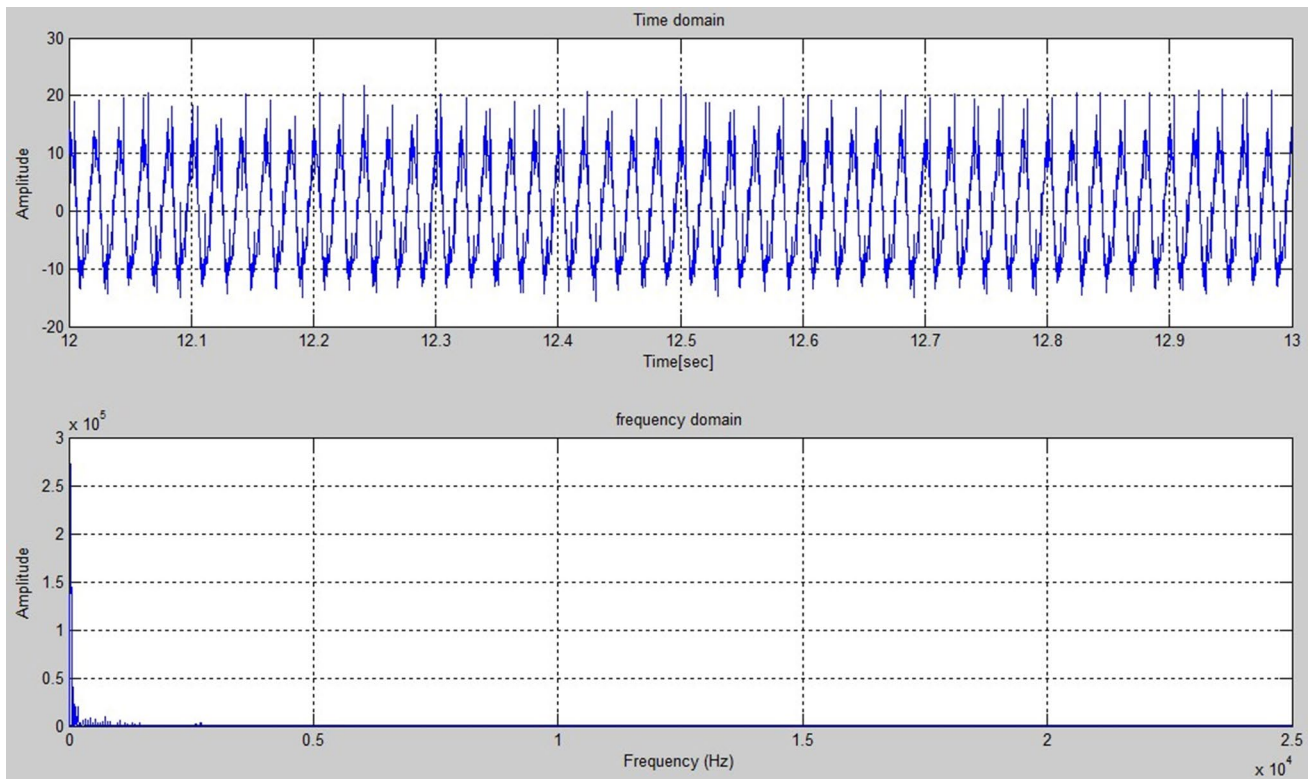


Fig. 19 Raw signal and frequency analysis at $N=23$ m/min, $f=350$ mm/min and $a=1.5$ mm, experiment 15

Table 9 Average surface roughness measurements

Experiment no.	MPs			Average surface roughness value <i>Ra</i> (μm)
	<i>N</i> (m/min)	<i>f</i> (mm/min)	<i>a</i> (mm)	
1	19	250	1.5	3.068
2	21	250	1.5	1.619
3	23	250	1.5	2.132
4	25	250	1.5	3.042
5	27	250	1.5	2.663
6	23	250	0.7	1.317
7	23	250	1	2.483
8	23	250	1.5	2.093
9	23	250	2	2.028
10	23	250	2.3	2.430
11	23	150	1.5	1.047
12	23	200	1.5	1.229
13	23	250	1.5	2.710
14	23	300	1.5	2.391
15	23	350	1.5	3.120

the minimum value was $Ra = 1.619 \mu\text{m}$ at $N = 21 \text{ m/min}$, as shown in Fig. 26.

As for the DC effect, Figs. 10, 11, 12, 13 and 14 express the DC effect on VS. The highest values of amplitude ranged from 5859 to 43,940 dB, and the related frequency values were 50, 100, and 200 Hz. Apart from these frequency values, steady machining was achieved throughout the frequency range up to 25,000 Hz. The maximum amplitude values in the time domain were 13.5 mm/s^2 for $a = 0.7, 1, 1.5,$ and 2 mm (experiments 6, 7, 8, and 9), then increased to 21.68 mm/s^2 at $a = 2.3 \text{ mm}$ (experiment 10). Figures 22 and 23 illustrate the relationship between VS amplitude and frequency and the DC. In Fig. 22, the highest value of the amplitude is at $a = 2.3 \text{ mm}$. In Fig. 23, all the DC values gave a frequency range from 50 to 100 to 200 Hz. As shown in Fig. 27, the maximum SR value was $Ra = 2.4838 \mu\text{m}$ at $a = 1 \sim 2.3 \text{ mm}$, and the minimum value was $Ra = 1.317 \mu\text{m}$ at $a = 0.7 \text{ mm}$.

However, for the FR effect, Figs. 15, 16, 17, 18 and 19 express the FR effect on the VS. The high amplitude values range from 584 to 41,000 dB, and the related frequency values start from 50 Hz up to 1187 Hz. The highest amplitude values appeared at 50, 100, and 150 Hz frequencies. By excluding these frequency values, steady machining was achieved throughout the frequency range up to 25,000 Hz. The maximum amplitude values in the time domain were 0.7767 mm/s^2 and 0.7056 mm/s^2 for $f = 150$ and 200 mm/min , respectively, 2.787 mm/s^2 for $f = 250 \text{ mm/min}$, 13.14 mm/s^2 for $f = 300 \text{ mm/min}$, and 21.67 mm/s^2 for $f = 350 \text{ mm/min}$, while N and a were kept constant at values ($N = 27 \text{ m/min}$, $a = 1.5 \text{ mm}$). Figures 24 and 25 illustrate the relationship between VS amplitude and

frequency and the FR. In Fig. 24, the amplitude values at $f = 150, 200,$ and 250 mm/min are much lower than the values at $f = 300$ and 350 mm/min . In Fig. 25, at $f = 300$ and 350 , the lower frequency values appeared (50–100 and 200 Hz), while other f values gave frequency values from 500 to 1300 Hz. The highest SR value was $Ra = 3.120 \mu\text{m}$ at $f = 350 \text{ mm/min}$, and the minimum value was $Ra = 1.047 \mu\text{m}$ at $f = 150 \text{ mm/min}$, as shown in Fig. 28.

Generally, the minimum VS amplitude values in both frequency and time domains were obtained at MPs' combinations related to experiments 11, 12, and 13. In these experiments, both N and a were kept at the values $N = 23 \text{ m/min}$, and $a = 1.5 \text{ mm}$, and the FR values were 150, 200, or 250 mm/min. These MPs' combinations resulted in the minimum SR values as well. $Ra = 1.047 \mu\text{m}$, and $Ra = 1.229 \mu\text{m}$ which are related to experiments 11 and 12, while the MPs related to experiment 13 resulted in a mean SR value of $Ra = 2.710 \mu\text{m}$, as explained in Table 9.

While the maximum VS amplitude values were obtained for MPs' combinations of ($N = 23 \text{ m/min}$, $f = 250 \text{ mm/min}$, and $a = 2.3 \text{ mm}$), and ($N = 23 \text{ m/min}$, $f = 350 \text{ mm/min}$, and $a = 1.5 \text{ mm}$). The first MPs' combination was related to experiment 10, where N and f were kept at their values ($N = 23 \text{ m/min}$ and $f = 250 \text{ mm/min}$), and the DC was at the highest proposed value $a = 2.3 \text{ mm}$. The second MPs combination was related to experiment 15, where N and a were kept at their values ($N = 23 \text{ m/min}$, and $a = 2.3 \text{ mm}$), and the FR was at the highest proposed value $f = 350 \text{ mm/min}$. Further, the maximum SR value ($Ra = 3.120 \mu\text{m}$) was obtained at the MPs' combination of experiment 15 ($N = 23 \text{ m/min}$, $f = 350 \text{ mm/min}$, and $a = 1.5 \text{ mm}$), which was related to the maximum VS values. Experiment 10 resulted in a mean SR value ($Ra = 2.430 \mu\text{m}$), which was related to maximum VS values too. Furthermore, experiments 1, 4, 7, and 13 had high SR values, with $Ra = 3.068 \text{ m}$, $Ra = 3.042 \text{ m}$, $Ra = 2.483 \text{ m}$, and $Ra = 2.710 \text{ m}$, respectively.

Discussion

SR measurement, characterization, and online prediction present a vital role in the enhancement of machining performance and the increase of machine automation. In order to ensure a machining process free of unwanted vibrations and with a good surface finish, this work focuses on an experimental investigation of the MPs' influence on VS and SR in the aluminum alloy AA5083 end milling operation. It also develops three ANN models for potential use in the online prediction of SR in a CNC milling machine. Different combination sets of the MPs (CS, DC, and FR) were used to assess each cutting parameter's effect individually on both the VS and SR. The results showed a significant

Table 10 Maximum amplitude values in both time and frequency domains and their related time and frequency values

Experiment no.	Property	Maximum amplitude values in both time and frequency domains and its related time and frequency values					
1	X [time]	12.06	12.39	12.55	12.63	12.71	12.99
	Y [Amplitude]	14.18	13.47	13.89	13.38	13.59	13.25
	X1 [frequency]	100	100.6	50	100.8	99.2	94.19
	Y1 [Amplitude]	3206	13,240	11,140	7866	7778	7404
2	X [time]	12.12	12.30	12.48	12.68	12.84	12.96
	Y [Amplitude]	12.72	12.63	13.03	12.75	12.60	11.71
	X1 [frequency]	100	100.6	101	50	200	100.6
	Y1 [Amplitude]	27,360	15,150	7542	6129	3435	15,400
3	X [time]	12.18	12.26	12.49	12.86	12.92	12.98
	Y [Amplitude]	13.77	13.36	13.82	12.67	13.63	12.32
	X1 [frequency]	100	100.7	50	200	50.26	300
	Y1 [Amplitude]	28,740	12,000	7749	4640	5856	3678
4	X [time]	12.08	12.22	12.54	12.72	12.84	12.96
	Y [Amplitude]	13.43	13.75	13.84	12.55	13.66	12.61
	X1 [frequency]	100	100.8	50	50.51	100.9	50.22
	Y1 [Amplitude]	29,650	11,400	10,610	5722	9405	8505
5	X [time]	12.1	12.38	12.50	12.58	12.84	12.96
	Y [Amplitude]	14.11	14.14	13.75	14.57	12.98	12.44
	X1 [frequency]	100	100.7	101	100.9	50	50.29
	Y1 [Amplitude]	28,570	15,010	8689	5100	10,860	8139
6	X [time]	12	12.2	12.46	12.70	12.98	12.70
	Y [Amplitude]	13.18	13.47	13.62	12.53	12.72	12.53
	X1 [frequency]	100	50	100.82	100.85	100.88	100.85
	Y1 [Amplitude]	28,830	9575	8337	8077	7015	8077
7	X [time]	12.21	12.37	12.53	12.77	12.83	12.93
	Y [Amplitude]	13.77	13	13.19	12.84	12.60	13.68
	X1 [frequency]	100	100.7	50	100.8	200	50.4
	Y1 [Amplitude]	28,850	11,340	9186	6422	4642	5324
8	X [time]	12.16	12.26	12.43	12.7	12.82	12.98
	Y [Amplitude]	13.5	12.44	12.52	12.65	12.88	12.54
	X1 [frequency]	100	99.33	50	99.17	100.8	50.36
	Y1 [Amplitude]	26,480	10,970	8805	7260	7787	5859
9	X [time]	12.17	12.22	12.42	12.48	12.68	12.76
	Y [Amplitude]	13.69	12.32	12.42	12.3	12.84	12.45
	X1 [frequency]	100	50	100.9	100.8	49.66	50.4
	Y1 [Amplitude]	25,240	9068	7324	8180	6214	5699
10	X [time]	12.09	12.23	12.39	12.56	12.86	12.98
	Y [Amplitude]	21.06	21.27	21.31	21.59	21.6	20.68
	X1 [frequency]	50	49.5	50.67	100	50.66	50.89
	Y1 [Amplitude]	29,420	15,880	10,740	42,800	11,000	43,940
11	X [time]	12.18	12.52	12.83	12.87	12.48	13
	Y [Amplitude]	0.6655	0.7205	0.6087	0.7767	0.5364	0.7265
	X1 [frequency]	822	1055	616	1187	1040	791
	Y1 [Amplitude]	1145	1078	856	629	672	629
12	X [time]	12.05	12.14	12.33	12.66	12.79	12.95
	Y [Amplitude]	0.6781	0.6662	0.7056	0.6457	0.6323	0.6218
	X1 [frequency]	822	616	791	1055	1187	511
	Y1 [Amplitude]	1346	1077	1069	942	786	584

Table 10 (continued)

Experiment no.	Property	Maximum amplitude values in both time and frequency domains and its related time and frequency values					
13	X [time]	12.12	12.16	12.24	12.48	12.53	12.66
	Y [Amplitude]	2.795	2.349	2.471	2.26	2.787	2.766
	X1 [frequency]	412	504	823	206	490	642
	Y1 [Amplitude]	5482	4794	4463	3684	2502	2472
14	X [time]	12.09	12.33	12.45	12.55	12.61	12.94
	Y [Amplitude]	11.76	12.2	12.28	12.26	12.51	13.14
	X1 [frequency]	100	50	100.7	200	51	300
	Y1 [Amplitude]	26,180	9313	8463	4701	4065	3786
15	X [time]	12.06	12.24	12.5	12.66	12.88	12.94
	Y [Amplitude]	20.52	21.67	21.66	21.01	20.45	21.14
	X1 [frequency]	50	50.47	50.64	100	100.5	150
	Y1 [Amplitude]	27,200	15,880	10,930	41,000	22,030	19,730

Fig. 20 Relation between CS and vibration amplitude. $a = 1.5 \text{ mm}$, $f = 250 \text{ mm/min}$, $N = 19, 21, 23, 25, 27 \text{ (m/min)}$

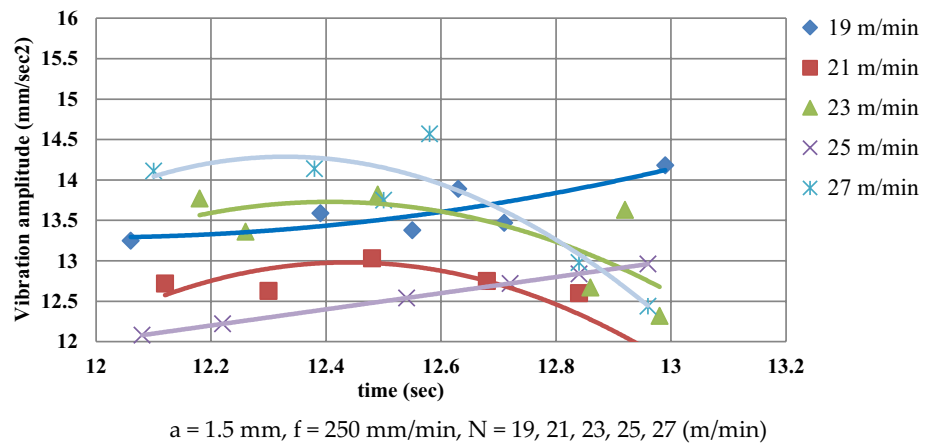
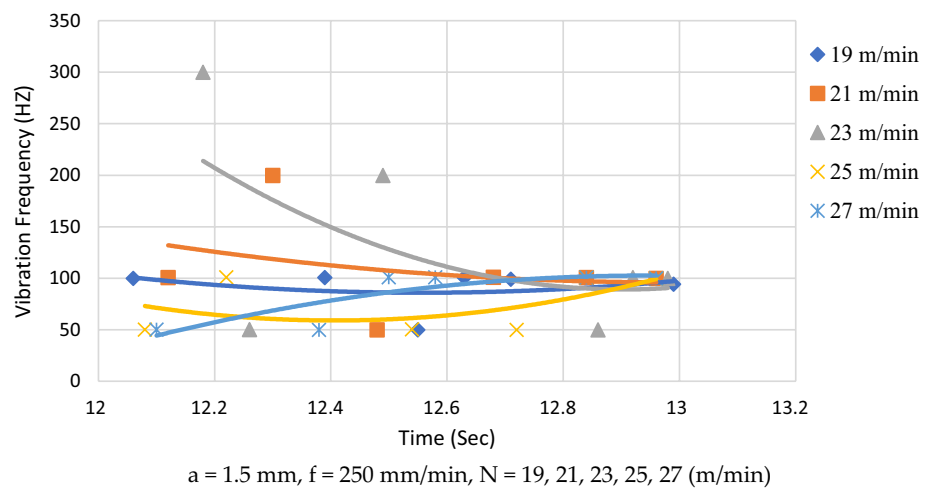


Fig. 21 Relation between CS and vibration frequency. $a = 1.5 \text{ mm}$, $f = 250 \text{ mm/min}$, $N = 19, 21, 23, 25, 27 \text{ (m/min)}$



relationship between both VS and SR, and the FR, then the DC, and finally the CS.

Increasing the CS while keeping the FR and DC constant at the selected mean values kept the VS amplitude values high through the proposed range (experiments 1, 2, 3, 4,

and 5). Further, SR values were high and nearly the same throughout the proposed range of CSs and experienced a slight decrease in experiment 5. The high VS and SR values may refer to the mean selected values for FR and DC used in these experiments (the interaction effect of the MPs).

Fig. 22 Relation between DC and vibration amplitude.
 $N=23$ m/min, $f=250$ mm/min,
 $a=0.7, 1, 1.5, 2, 2.3$ (mm)

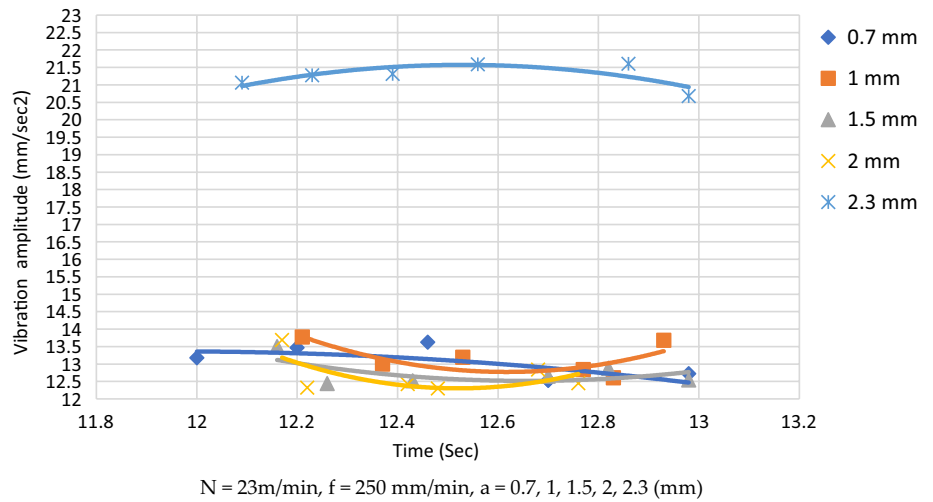


Fig. 23 Relation between DC and vibration frequency.
 $N=23$ m/min, $f=250$ mm/min,
 $a=0.7, 1, 1.5, 2, 2.3$ (mm)

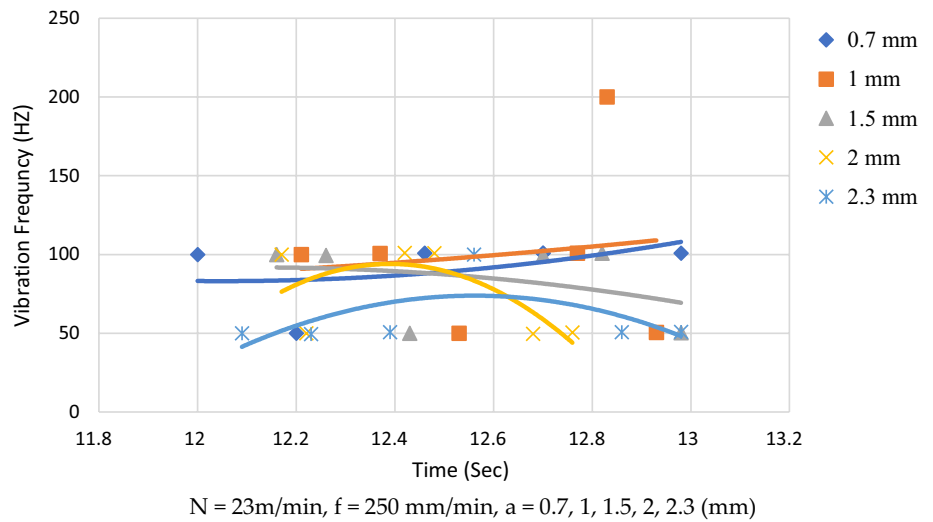


Fig. 24 Relation between FR and vibration amplitude.
 $N=23$ m/min, $a=1.5$ mm,
 $F=150, 200, 250, 300, 350$ (mm/min)

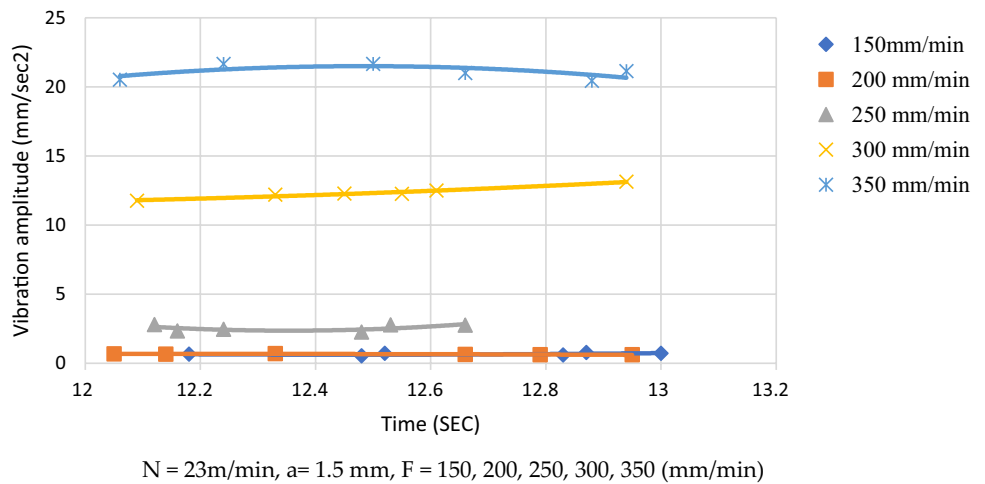


Fig. 25 Relation between FR and vibration frequency. $N=23$ m/min, $a=1.5$ mm, $F=150, 200, 250, 300, 350$ (mm/min)

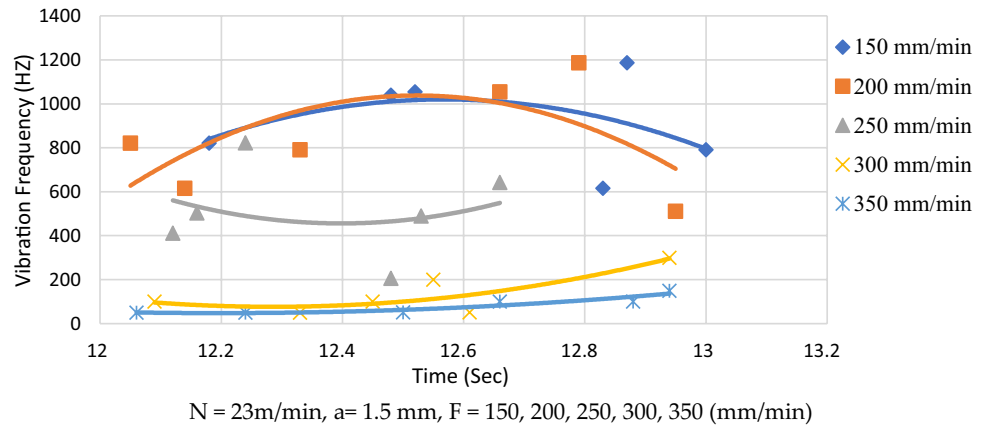


Fig. 26 Effect of CS on surface roughness. $a=1.5$ mm, $f=250$ mm/min, $N=19, 21, 23, 25, 27$ m/min

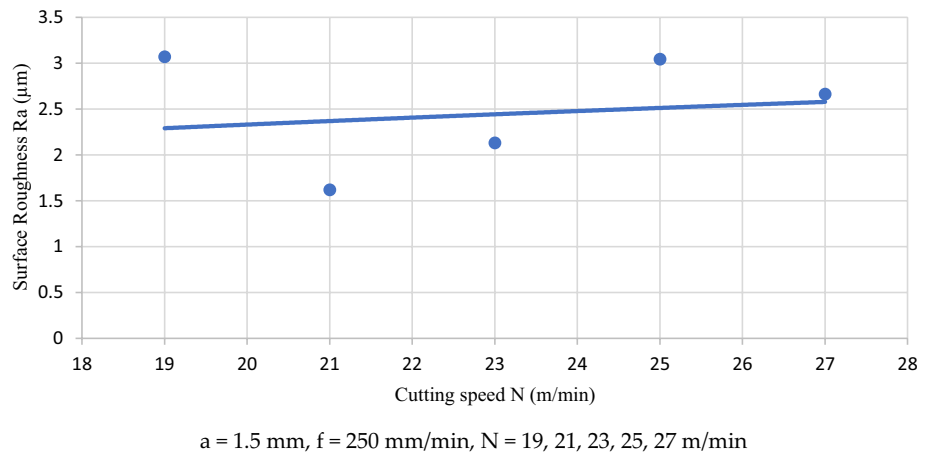
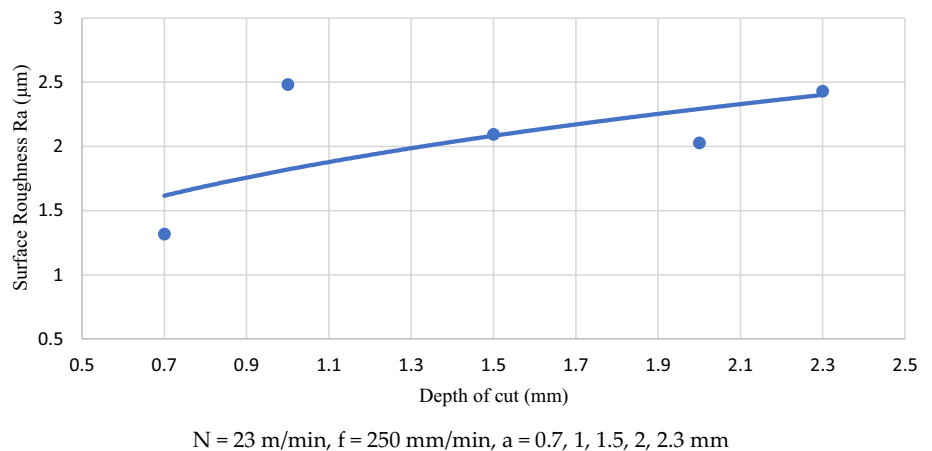


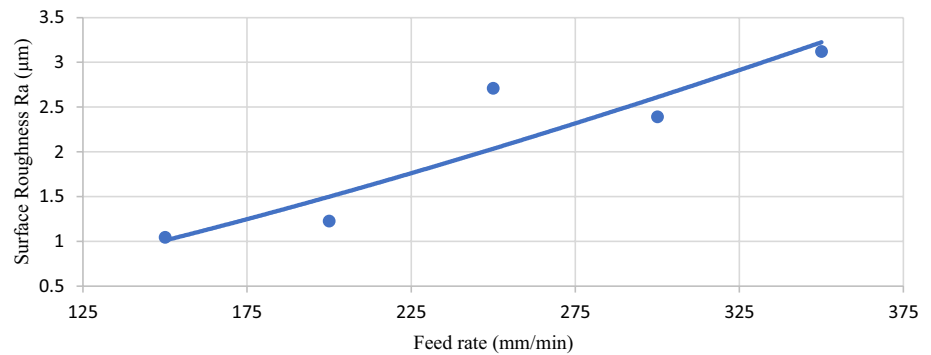
Fig. 27 Effect of DC on surface roughness. $N=23$ m/min, $f=250$ mm/min, $a=0.7, 1, 1.5, 2, 2.3$ mm



As seen in experiments 6 through 10, the increase in the DC had a substantial influence on the VS amplitude values and SR values. Increasing DC while keeping FR and CS at mean values resulted in a continuous increase in VS and SR until they reached their maximum values when DC was at its maximum value. In addition, increasing the FR values had a significant effect on the VS amplitude values and SR

values, as in experiments 11, 12, 13, 14, and 15. The minimum FR values associated with experiments 11, 12, and 13 yielded the minimum VS amplitude in the time domain and frequency domain values as well as the minimum SR values. While the maximum VS amplitude values and SR values were obtained in experiments 10 and 15, the DC and FR were at their highest proposed values. Hence, both FR and

Fig. 28 Effect of FR on surface roughness. $N=23$ m/min, $a=1.5$ mm, $f=150, 200, 250, 300, 350$ mm/min



DC had a more substantial influence on VS and SR values than spindle CS in the proposed range, as changing each one of them though keeping the other two MPs constant led to a significant change in VS values and SR values. In general, the rise in DC and FR results in a rise in VS amplitude values and SR values, while the increase in CS led to an increase in VS amplitude values and a decrease in SR values.

This is similar to what has been found in previous investigations presented by numerous researchers: using a multiple regression model, Lou et al. estimated the SR in aluminum 6061 milling with a four flute high-speed steel cutter tool in [2]. They claimed that by using CS, FR, DC, and their interactions, the SR is accurately expected. The FR was the highest important MP for SR prediction. Response surface modeling was used by Arokiadass et al. in [11] to study SR in the milling of Al/SiCp metal matrix composites by carbide-based tool. They found that the SR will significantly decrease with the increase in CS, and the SR will increase with the FR increase. A slight increase in SR resulted from increasing the DC. High CS, low DC, and low FR will achieve the best SR. In the literature [49], Ravi kumar D. Patel et al. predicted the SR in the CNC milling of Aluminum using HSS CNC milling cutters and modified the MPs using ANN. They found that the SR is influenced mostly by the FR, then the CS, and lastly the DC. This arrangement of parameter significance disagrees with this study (FR, then DC, and lastly CS). This can be referred to the different Aluminum material alloys used, the different cutting tool used, or the different cutting conditions range used, or taking all parameters interaction into consideration by them.

Other researchers reported further notes while turning different steel alloys; for the steel 9SMnPb28K (DIN) turning utilizing carbide inserts TPUN 160,308 P10 (ISO), Davin in the investigations [50] examined the influence of

cutting condition on SR using multiple linear regression. He indicated that CS, followed by FR, and then the interaction of both CS and FR had a substantial influence on SR. Whereas the DC, the interaction of both CS/DC and FR/DC, had no substantial influence on SR. The disagreement could be due to a change in material, the machining operation used (turning and milling are different), or the interaction effect of the MPs. Davim and Figueira in the literature [51] compared the machining forces, SR, and tool wear of traditional and wiper ceramic tools when turning AISI D2 steel. They came to the conclusion that FR had the greatest statistical impact on SR and that SR grows with cutting time and primarily with FR. For this range of MPs, the relationship of SR with CS is unclear. In the researches [52], Ibraheem et al. used ANN to forecast tool wear for cold-drawn plain carbon steel turning with a square carbide insert tool (grade P25). They claimed that the VS amplitude was significantly affected by the DC and tool wear. The VS amplitude increases somewhat as the DC increases, and the vibration frequency is not significantly affected by the change in DC. As CS rises, VS amplitude rises as well. The VS frequency changes are not influenced by the state of the flank wear or the cutting conditions, but rather by the tool holder's natural frequency, and the FR has a negligible impact on the VS amplitude. When turning free machining steel using a carbide tool, Gaitonde et al. [53] used the Taguchi technique and utility concepts to enhance the MPs with the goal of minimizing SR and maximizing the metal removal rate. According to their findings, CS and DC are the two MPs that have the most impact on the optimization of multiple performance criteria. And in order to concurrently reduce SR and increase the material removal rate, a group of greater levels of CS, DC, and FR at the middle level is essential. However, the SR rises with a rise in FR, as the SR is proportionate to the FR square. The

disagreement may come up from studying the optimization of multiple criteria and cutting parameter interactions.

There are some limitations to this study, such as, it concentrated on Aluminum AA5083 alloy end milling, and a proposed range of MPs was used. Experimental measurements were applied in the feed direction only. The machining operation used in the experiments is milling only. The study also concentrated on the SR performance criteria based on MPs and VS measurements. The effect of each parameter was studied individually, keeping the other two parameters constant at mean values. Parameter interactions were not studied in depth. Optimization of multiple criteria was not taken into account.

The implication and significance of the study are that although many investigations have been done to predict SR based on MPs, a small number of investigations have taken VS into account. Hence, SR could be predicted based on the MPs and VS measurements and save a lot of effort to get a good surface finish without unwanted vibration and with good machining criteria.

Development and Validation of ANN Models of Vibration Signal Measurement and Surface Roughness

In this research, three models of ANN were established to properly infer VS level and SR related to MPs' conditions during milling operations and led to stable machining and good surface quality. The first ANN model was developed and optimized with the CS, FR, and DC as inputs and the frequency and amplitude of the VS as outputs. The second ANN model was developed with the CS, FR, and DC as inputs and the SR value as the output. The third ANN model was established with the CS, FR, and DC, the frequency and amplitude of VS as inputs, and the SR value as the output. ANN models were established and trained by applying the MATLAB 2018a software package, with a feed-forward architecture and the supervised learning technique of the backpropagation Levenberg Marquardt algorithm, with a sigmoid activation function. Three layers; input, output, and hidden were proposed, with 8 (in the first ANN model) or 10 (in the second and third ANN models) neurons in the hidden layers. Figure 29a–c shows the structure diagrams of the ANN models proposed to predict VS, SR (when the MPs are used as inputs), and SR (when the MPs, vibration frequency, and amplitude are used as inputs).

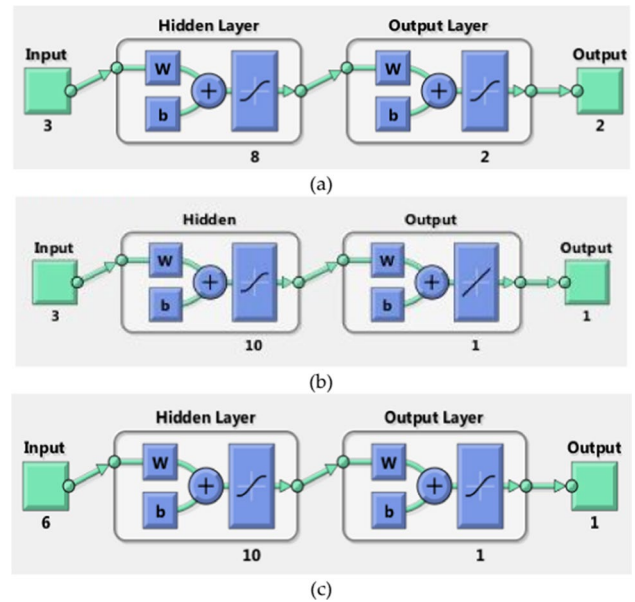


Fig. 29 Structure diagram of: **a** The first ANN model (vibration signal), **b** The second ANN model (SR), **c** The third ANN model (SR)

The measured data are separated into three groups: the training data set (70%), the validation data set (15%), and the testing data set (15%). All the training set of data is introduced to the ANN for learning, and the weights are updated after each epoch of the presentation of the data. In general, the training does not stop until a training error is reached or a certain number of iterations are finished. The network performance evaluation is carried out at this step by the comparison between the expected outputs related to the presented inputs with the experimentally measured values.

The network performance has been tested irregularly, at one thousand iterations, against the testing set. When generalization stops improving, the training automatically ends, as demonstrated by an increase in the validation data mean-squared error. Numerous architectures of ANN have been checked to get the best performance. In the different training runs, initial weights were taken as random numbers ranging from -1 to $+1$. The training took place on a PC for several minutes.

Figure 30 shows the ANN training using the nntain tool in the three developed ANN models. In Fig. 31, the ANNs regression for training, validating, and testing the model is illustrated. The solid line denotes the ideal fit, whereas the broken line denotes the best line fit (output equals targets). Because the experimental and predicted values are so

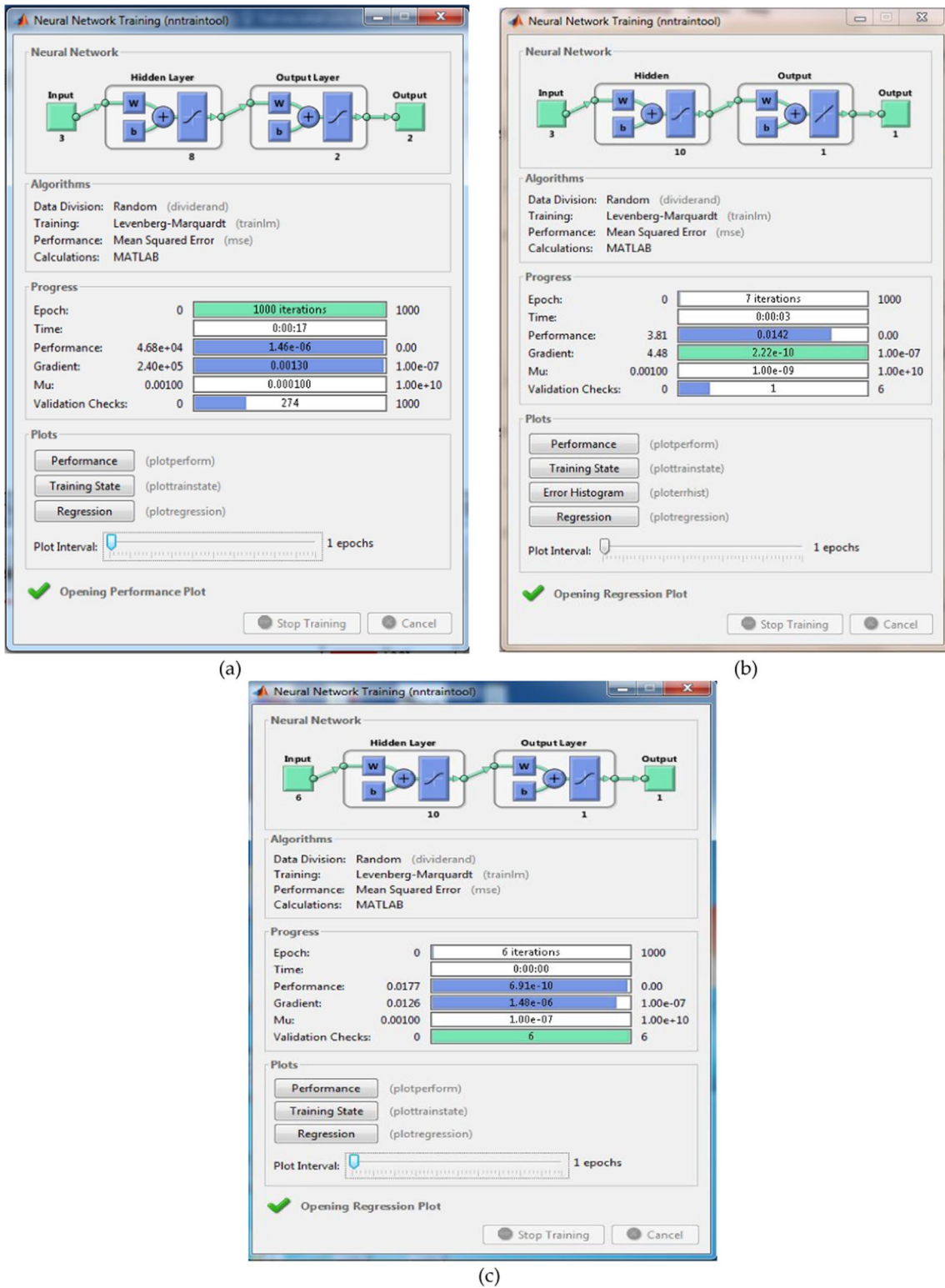
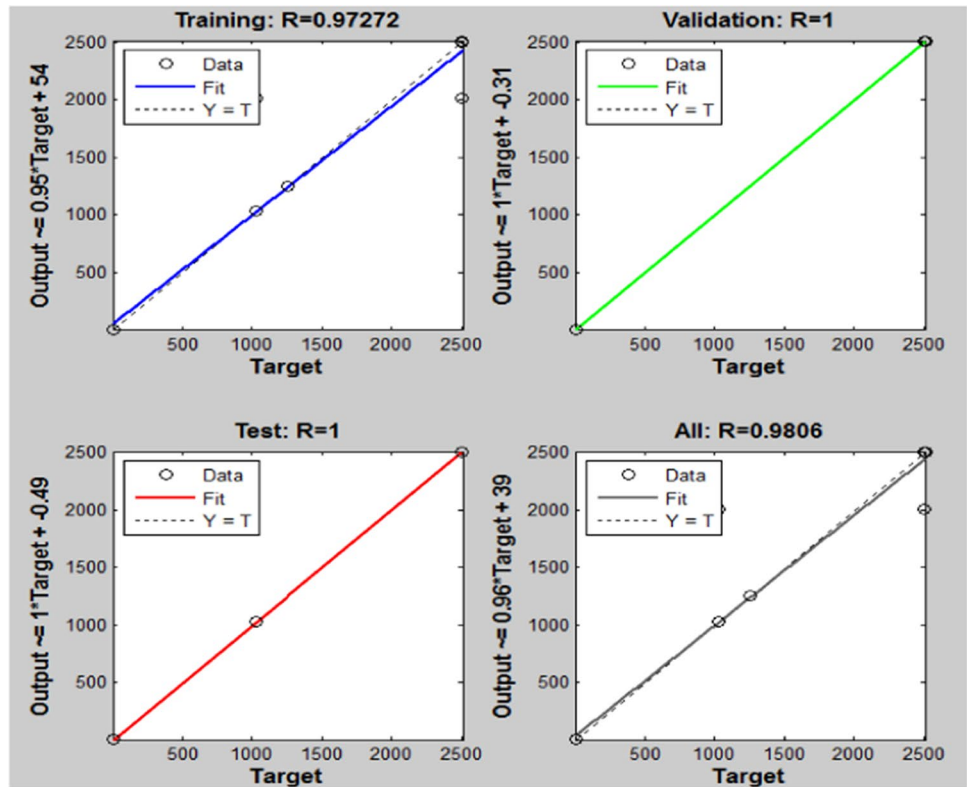
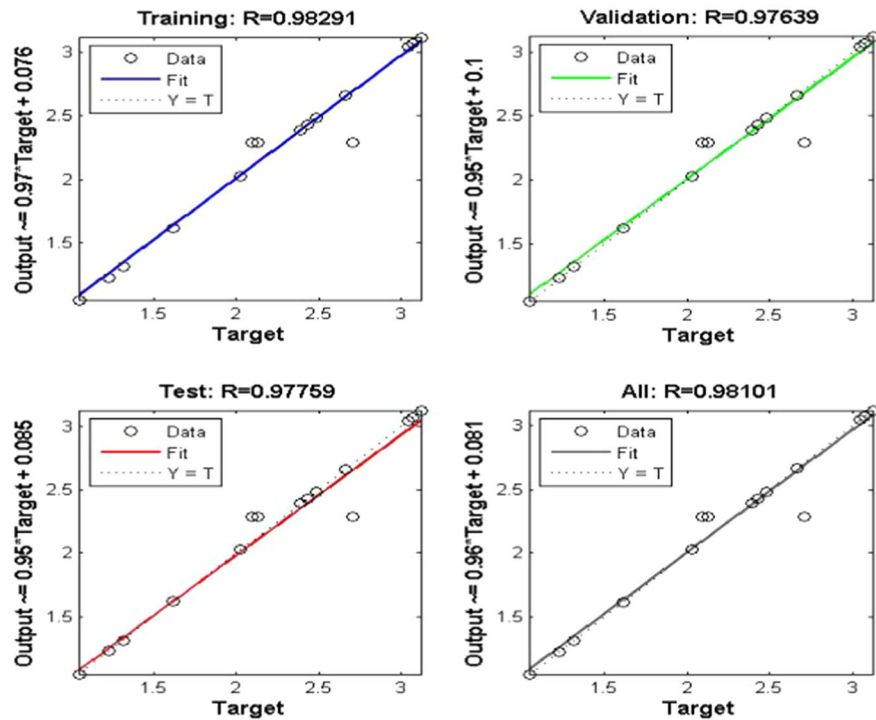


Fig. 30 ANN training: **a** The first ANN model (vibration signal), **b** The second ANN model (SR), **c** The third ANN model (SR)

Fig. 31 Regression plot: **a** The first ANN model (vibration signal), **b** The second ANN model (SR), **c** The third ANN model (SR)

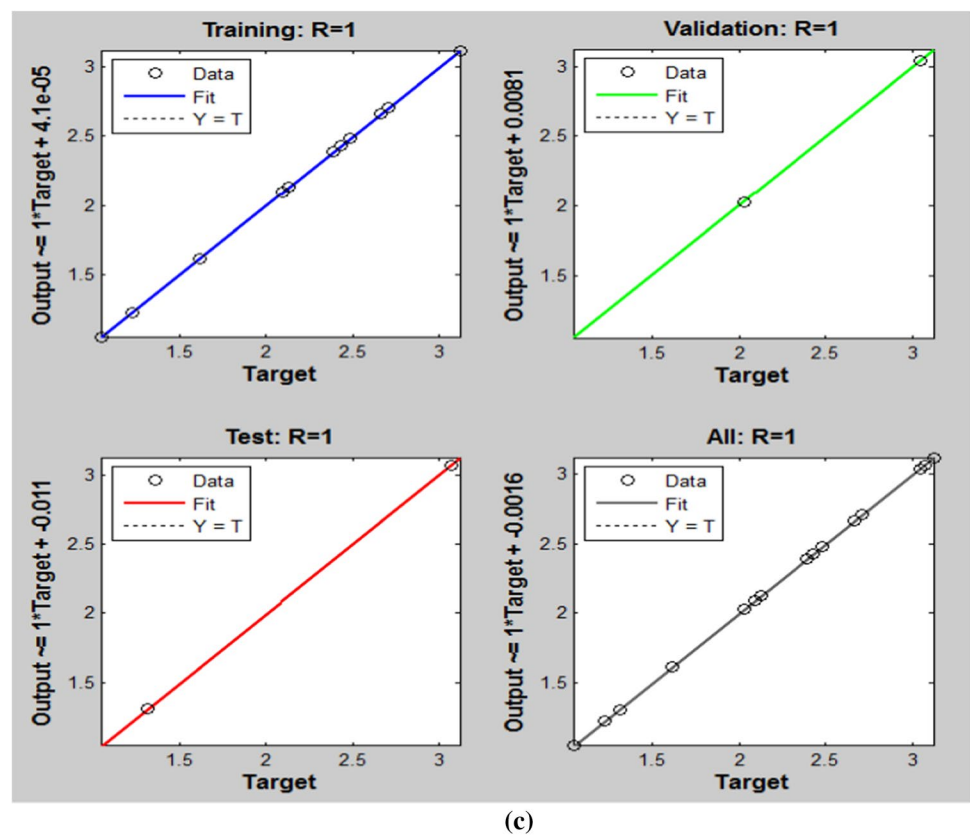


(a)



(b)

Fig. 31 (continued)



similar, the suggested ANN models have a strong correlation factor for VS and SR prediction.

The performance plot is presented in Fig. 32 for the training, validation, and test sets, expressed in terms of mean-squared error and shown on a log scale. The first ANN model reached its best performance of 0.27433 at 726 epochs. While the second ANN model reached 0.018899 at 6 epochs, the third ANN model reached 0.018487 at 9 epochs.

The developed ANN models are validated and tested, and the results are displayed in Figs. 33, 34, 35 and 36. The measured data is compared to the output data of the trained ANNs for the same inputs. Figures 33 and 34 show the measured vibration amplitude and frequency compared to the output vibration amplitude and frequency of the trained first ANN to the same inputs (MPs' combinations) from experiments 1–15. Figure 35 shows the measured SR compared to the ANN output SR of the trained second ANN for the same inputs (MPs' combinations) from experiments 1–15. Figure 36 shows the measured SR compared to the output SR of the trained third ANN for the same inputs (MPs' combinations and vibration amplitude

and frequency) from experiments 1–15. The trained results are close to the measured results in the three ANN models. The results of the training show that the ANN is capable of reproducing the experimental data with acceptable accuracy. The third ANN presented better results than the second ANN, indicating that using the VS in combination with the MPs enhances the modeling and prediction of SR using ANN.

Similar observations were reported by different researchers; in the literature [32], Antonio Vallejo used ANN to forecast the SR in peripheral milling; all ANN architectures had extremely low prediction errors and good performance when it came to machining various aluminum alloys and cutting tools. The wiper ceramic and traditional inserts in the turning of AISI D2 cold-worked steel through ANN were compared by Vinayak Gaitonde et al. [54]. It was shown that ANN models can be used to evaluate the performance of both ceramic inserts in terms of machinability and to analyze the effects of cutting conditions effectively. In the researches [28], Azlan Mohd Zain et al. predicted the SR of the Ti-6Al-4 V alloy in end milling machining using ANN.

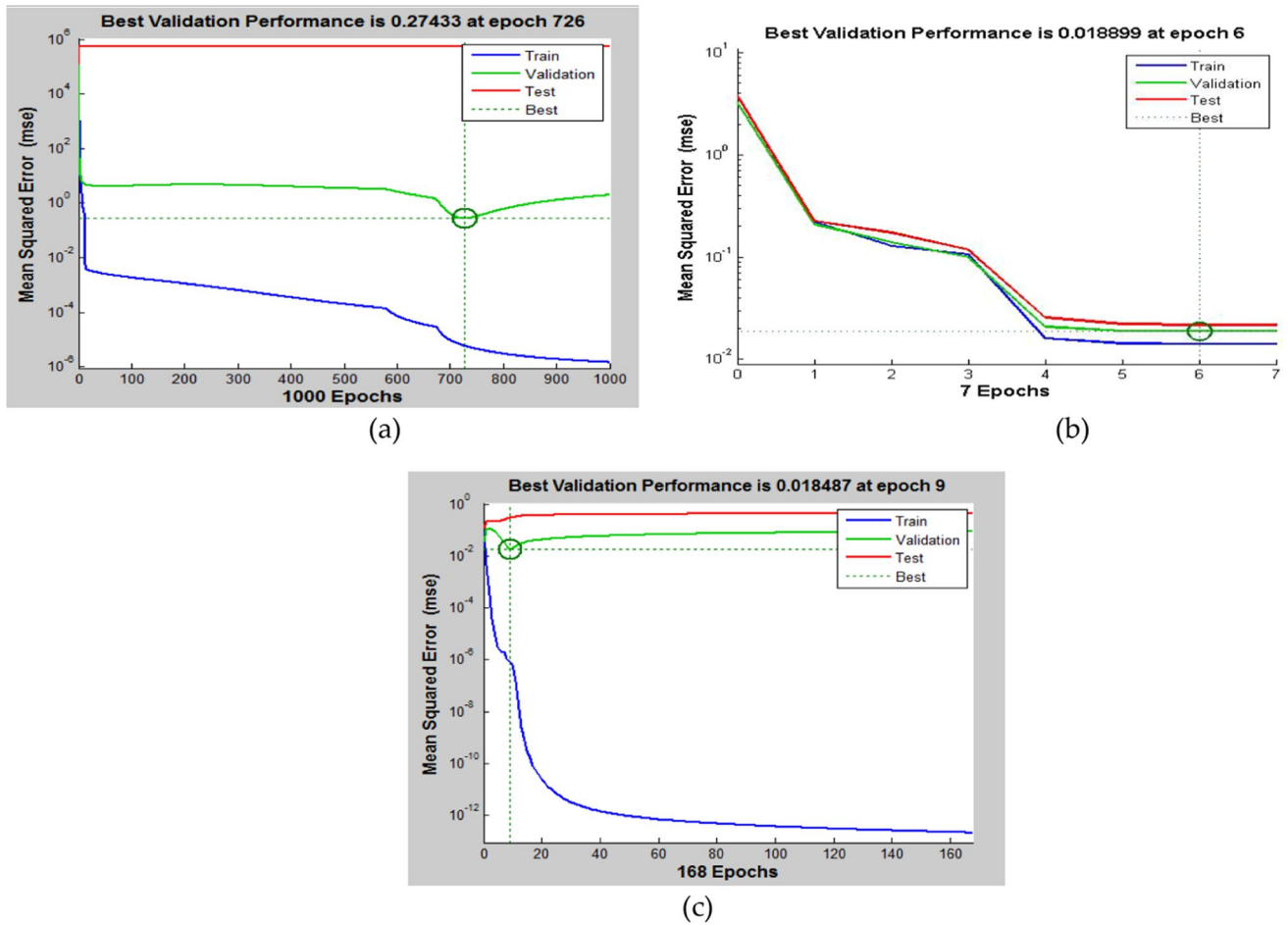


Fig. 32 Performance plot: **a** The first ANN model (vibration signal), **b** The second ANN model (SR), **c** The third ANN model (SR)

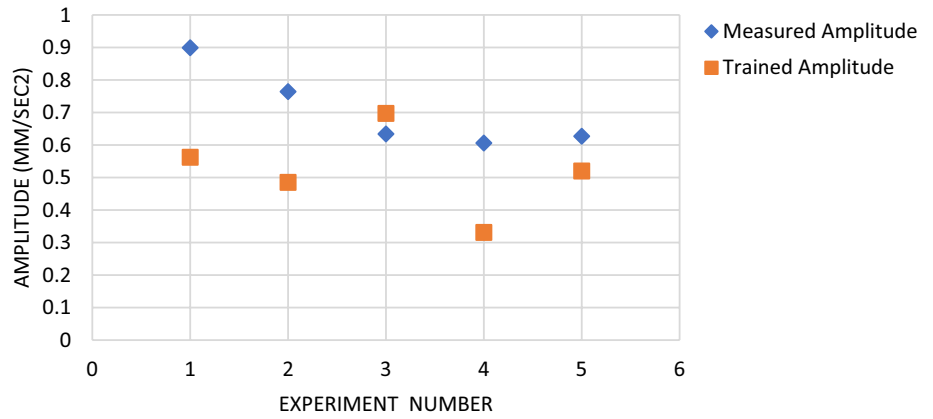
They concluded that the SR model could be enhanced by changing the layers and nodes’ numbers in the hidden layers, which carried out an accurate performance evaluation by small training data samples. In the literature [31], Abdel Badie Sharkawy used three different forms of artificial networks to estimate the SR of end milling aluminum 6061 alloy. It has been determined that the radial basis function network model provides the highest prediction accuracy. Monitoring tool wear by investigating the tool’s vibration amplitude was carried out using a multilayer ANN system created by Ibraheem et al. [52]. The number of iterations, the error level, the learning rate, and the momentum parameter of several ANN topologies have been tested. The training results demonstrate that the ANN can satisfactorily replicate the experimental data. In the literature [5], Wu and Lei used VS analysis and ANN to forecast the SR of S45C

steel during the milling process. They discovered that the vibration performance throughout the milling operation, in addition to the MPs, has an impact on the SR. As a result, the characteristics of VS are used to improve the accuracy of SR predictions.

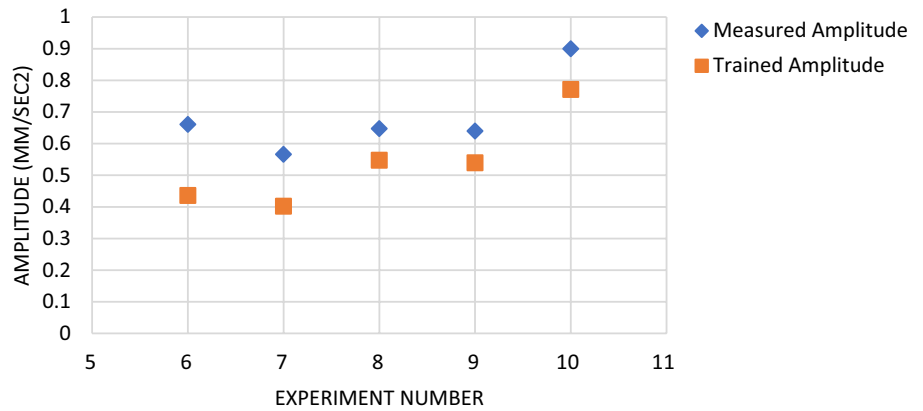
Conclusions

The vibration signal and surface roughness of AA5083 alloy end milling were studied using 15 experiments under the proposed machining parameters’ combinations. The influence of each machining parameter on both vibration signal values and surface roughness were studied separately, whereas the other parameters were kept constant at a

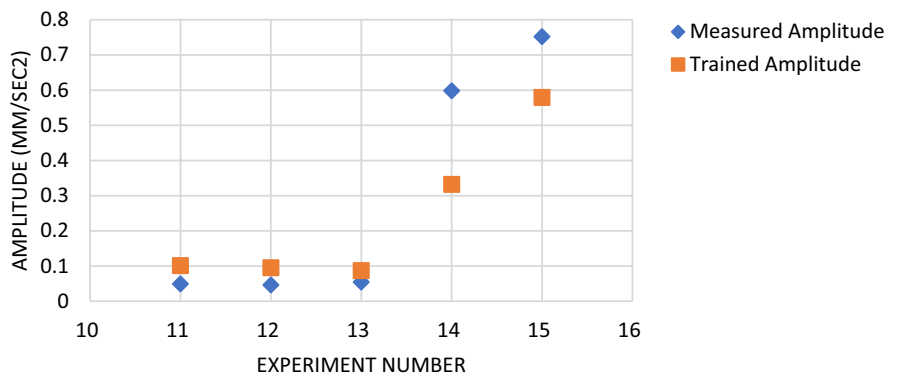
Fig. 33 Measured and trained results of vibration amplitude using the first ANN model: **a** In experiments 1–5, **b** In experiments 6–10, **c** In experiments 11–15



(a)



(b)



(c)

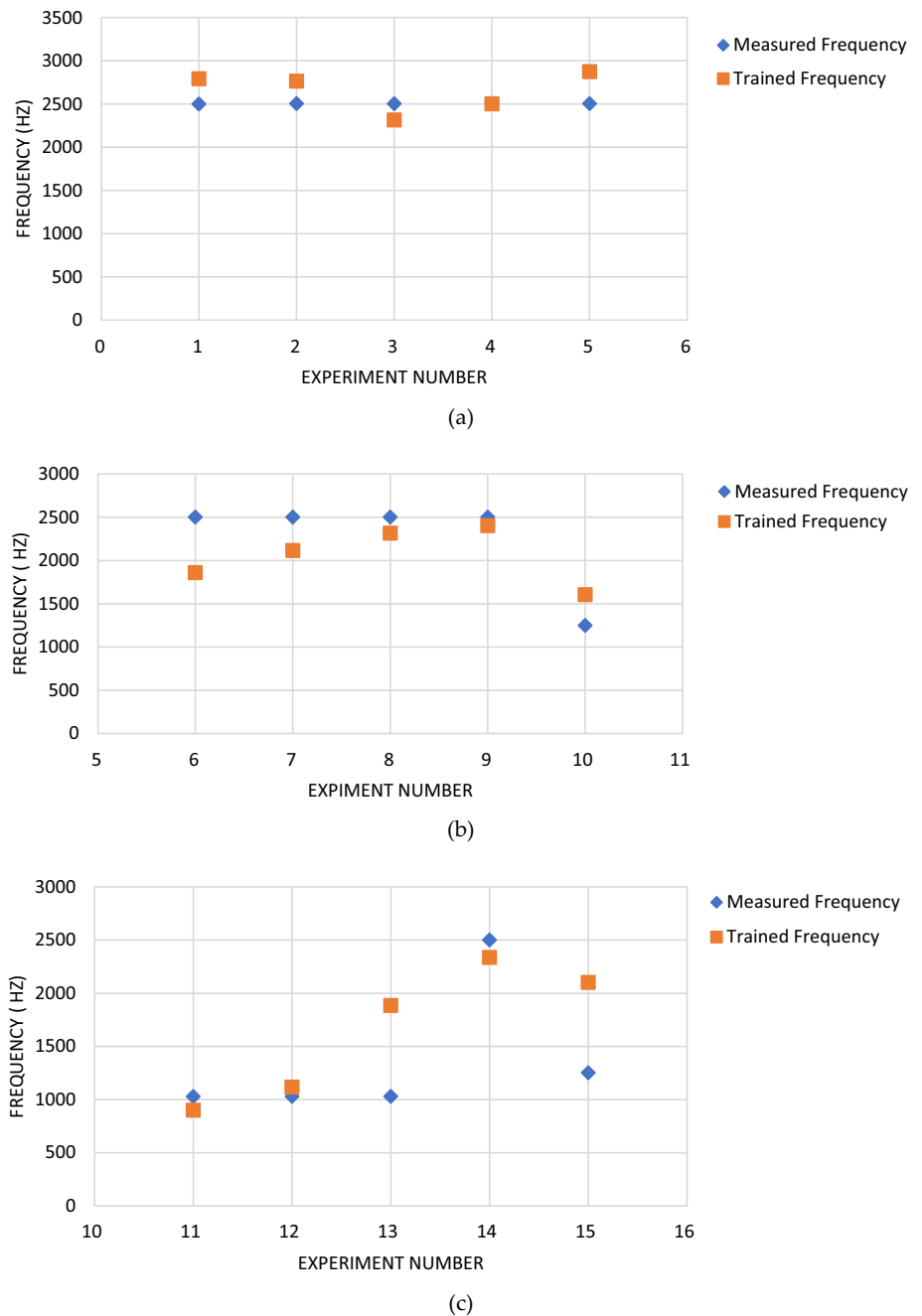
selected value. Artificial neural network technique is used in the modeling and prediction of both surface roughness and vibration signal.

The findings support that the rise in cutting speed, depth of cut, and feed rate led to a rise in vibration signal level values. Also, surface roughness values get higher with the

rise in depth of cut and feed rate, and get lower with the rise in cutting speed. Both feed rate and depth of cut had a more substantial influence on vibration values and surface roughness values than cutting speed.

Cutting Parameters' combinations related to minimum and maximum vibration levels and surface roughness were

Fig. 34 Measured and trained results of vibration frequency using the first ANN model: **a** In experiments 1–5, **b** In experiments 6–10, **c** In experiments 11–15

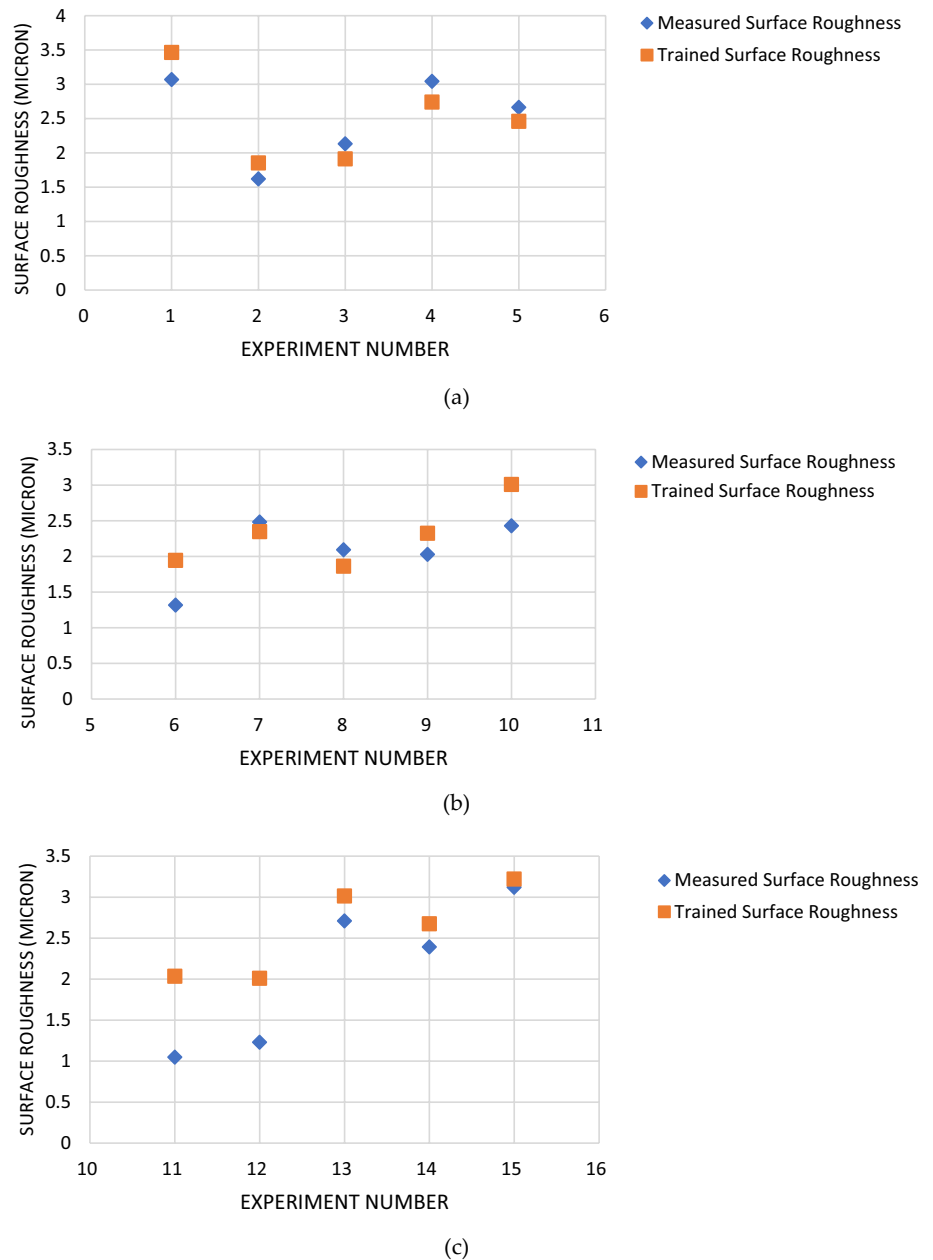


assigned. The cutting parameters that result in low vibration levels are a cutting speed of 23 m/min, depth of cut of 1.5 mm, and feed rate values of 150, 200, or 250 mm/min, which lead to a low surface roughness of 1.047 μm . While the maximum vibration values were obtained at ($N=23$ m/min, $f=250$ mm/min, and $a=2.3$ mm) and ($N=23$ m/min, $f=350$ mm/min, and $a=1.5$ mm) machining parameter combinations, the maximum surface roughness value ($R_a=3.120$ μm) was obtained at cutting

parameter combinations ($N=23$ m/min, $f=350$ mm/min, and $a=1.5$ mm), which was related to the maximum vibration values.

Three artificial neural networks with one hidden layer that consists of eight or ten neurons were successfully used to predict the vibration signal and surface roughness. The artificial neural network models showed a reasonable agreement with the experimental results. Vibration levels and surface roughness can be controlled using the

Fig. 35 Measured and trained results of SR using the second ANN model: **a** In experiments 1–5, **b** In experiments 6–10, **c** In experiments 11–15

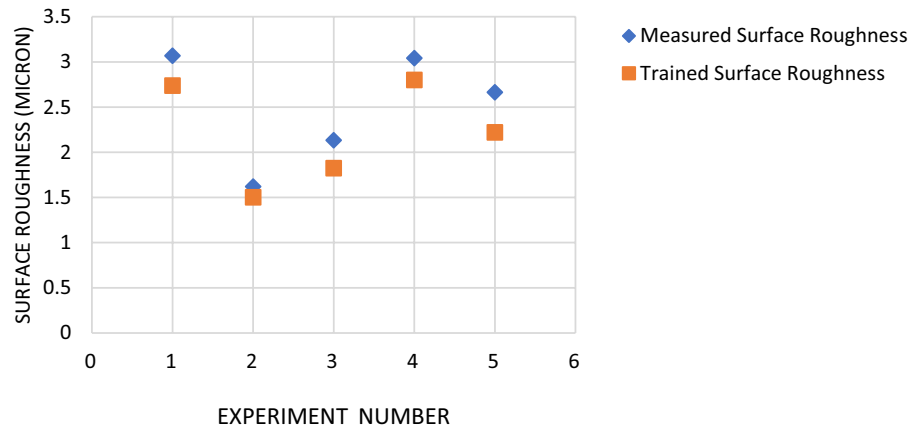


developed artificial neural network models that represent a guide for operators in selecting the proper cutting speed, feed rate, and depth of cut that guarantees stable cutting with acceptable surface quality. Taking the vibration signal into account enhances the ability of the artificial neural network to infer the surface roughness for different cutting conditions.

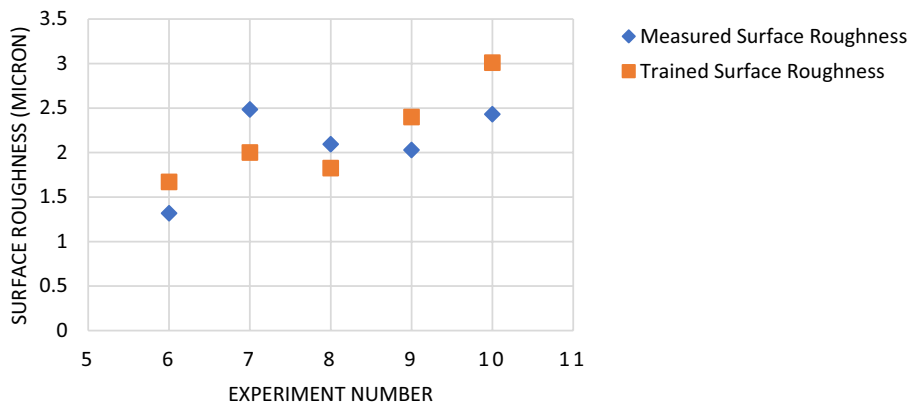
However, these findings may be related to certain machining operations, specific materials, cutting tools, and proposed cutting parameter ranges. In future research work,

different neural network types, such as adaptive neuro-fuzzy inference systems, genetic-based fuzzy inference systems, radial basis neural networks, or other artificial intelligence techniques could be used in surface roughness and vibration level model prediction. The developed models may be used to build an adaptive control system for online monitoring, prediction, and control of both surface roughness and vibration level. Optimization of multiple criteria (such as surface roughness, material removal rate, etc.) and cutting parameters' interactions may be taken into account.

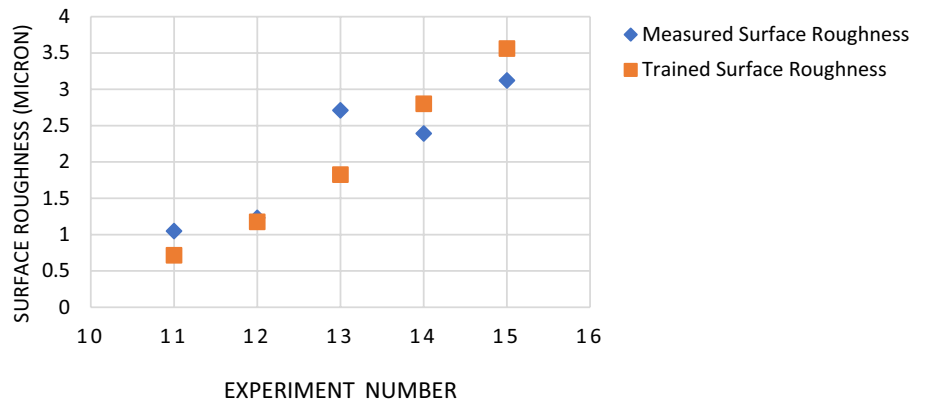
Fig. 36 Measured and trained results of SR using the third ANN model: **a** In experiments 1–5, **b** In experiments 6–10, and **c** In experiments 11–15



(a)



(b)



(c)

Funding No funding.

Declarations

Conflict of interest The authors declare no conflict of interest.

References

1. J.P. Davim, Ed., *Machining Fundamentals and Recent Advances*, First edition © 2008 Springer-Verlag London Limited. <https://doi.org/10.1007/978-1-84800-213-5>.
2. M.S. Lou, J.C. Chen, C.M. Li, Surface roughness prediction technique for CNC end-milling. *J. Ind. Technol.* November 1998 to January 1999, **15**(1)

3. J.P. Davim, Ed., *Surface Integrity in Machining*, First edition[©], Springer-Verlag London Limited 2010. <https://doi.org/10.1007/978-1-84882-874-2>.
4. G. Boothroyd, W.A. Knight, *Fundamentals of Machining and Machine Tools*, Second edition. (Marcel Dekker Inc., New York, 1989)
5. T.Y. Wu, K.W. Lei, Prediction of surface roughness in milling process using vibration signal analysis and artificial neural network'. *Int. J. Adv. Manuf. Technol.* **102**, 305–314 (2019). <https://doi.org/10.1007/s00170-018-3176-2>
6. V.M. Huynh, Y. Fan, Surface-texture measurement and characterization with applications to machine-tool monitoring. *Int. J. Adv. Manuf. Technol.* **7**, 2–10 (1992). <https://doi.org/10.1007/BF02602945>
7. M. Brezocnik, M. Kavocic, M. Ficko, Prediction of surface roughness with genetic programming. *J. Mat. Process. Technol.* **157–158**, 28–36 (2004). <https://doi.org/10.1016/j.jmatprotec.2004.09.004>
8. P.G. Bernardos, G.-C. Vosniakos, Predicting surface roughness in machining: a review. *Int. J. Mach. Tools Manuf.* **43**(8), 833–844 (2003). [https://doi.org/10.1016/S0890-6955\(03\)00059-2](https://doi.org/10.1016/S0890-6955(03)00059-2)
9. J.P. Davim, Ed., *Design of Experiments in Production Engineering*, First edit. Switzerland: © Springer International Publishing 2016. <https://doi.org/10.1007/978-3-319-23838-8>.
10. J.P. Davim, Ed., *Statistical and Computational Techniques in Manufacturing*, First edit. © Springer-Verlag Berlin Heidelberg 2012. <https://doi.org/10.1007/978-3-642-25859-6>.
11. R. Arokiadass, K. Palaniradj, N. Alagumoorthi, Surface roughness prediction model in end milling of Al/SiCp MMC by carbide tools. *Int. J. Eng. Sci. Technol.* **3**(6), 78–87 (2011)
12. D.R. Patel, M.B. Kiran, V. Vakharia, Modeling and prediction of surface roughness using multiple regressions: a noncontact approach. *Eng. Rep.* **2**, e12119 (2020). <https://doi.org/10.1002/eng2.12119>
13. K. Bouacha, M.A. Yaltese, T. Mabrouki, J.-F. Rigal, Statistical analysis of surface roughness and cutting forces using response surface methodology in hard turning of AISI 52100 bearing steel with CBN tool. *Int. J. Refract Metal Hard Mater.* **28**(3), 349–361 (2010). <https://doi.org/10.1016/j.ijrmhm.2009.11.011>
14. D. Singh, P.V. Rao, A Surface roughness prediction model for hard turning process. *Int. J. Adv. Manuf. Technol.* **32**(11–12), 1115–1124 (2007). <https://doi.org/10.1007/s00170-006-0429-2>
15. S. Agarwal, P. VenkateswaraRao, Modeling and prediction of surface roughness in ceramic grinding. *Int. J. Mach. Tools Manuf.* **50**(12), 1065–1076 (2010). <https://doi.org/10.1016/j.ijmachtools.2010.08.009>
16. A.M. Zain, H. Haron, S. Sharif, Prediction of Surface roughness in the endmilling machining using Artificial Neural Network. *Expert Syst. Appl.* **37**(2), 1755–1768 (2010). <https://doi.org/10.1016/j.eswa.2009.07.033>
17. J.F. Briceno, H. El-Mounayri, S. Mukhopadhyay, Selecting an artificial neural network for efficient modeling and accurate simulation of the milling process. *Int. J. Mach. Tools Manuf.* **42**(6), 663–674 (2002). [https://doi.org/10.1016/S0890-6955\(02\)00008-1](https://doi.org/10.1016/S0890-6955(02)00008-1)
18. D. Karayel, Prediction and control of surface roughness in CNC lathe using artificial neural network. *J. Mater. Process. Technol.* **209**(7), 3125–3137 (2009). <https://doi.org/10.1016/j.jmatprotec.2008.07.023>
19. E.S. Topal, The role of stepover ratio in prediction of surface roughness in flat end milling. *Int. J. Mech. Sci.* **51**(11–12), 782–789 (2009). <https://doi.org/10.1016/j.ijmecsci.2009.09.003>
20. C. Lu, Study on prediction of surface quality in machining process. *J. Mater. Process. Technol.* **205**(1–3), 439–450 (2008). <https://doi.org/10.1016/j.jmatprotec.2007.11.270>
21. O. Colak, C. Kurbanoglu, M.C. Kayacan, Milling surface roughness prediction using evolutionary programming methods. *Mater. Des.* **28**(2), 657–666 (2007). <https://doi.org/10.1016/j.matdes.2005.07.004>
22. S.S. Roy, Design of genetic-fuzzy expert system for predicting surface finish in ultra-precision diamond turning of metal matrix composite. *J. Mater. Process. Technol.* **173**(3), 337–344 (2006). <https://doi.org/10.1016/j.jmatprotec.2005.12.003>
23. H. Oktem, T. Erzurumlu, F. Erzincanli, Prediction of minimum surface roughness in end milling mold parts using neural network and genetic algorithm. *Mater. Des.* **27**(9), 735–744 (2006). <https://doi.org/10.1016/j.matdes.2005.01.010>
24. S.P. Lo, An adaptive-network based fuzzy inference system for prediction of workpiece Surface roughness in end milling. *J. Mater. Process. Technol.* **142**(3), 665–675 (2003). [https://doi.org/10.1016/S0924-0136\(03\)00687-3](https://doi.org/10.1016/S0924-0136(03)00687-3)
25. W.-H. Ho, J.-T. Tsai, B.-T. Lin, J.-H. Chou, Adaptive network-based fuzzy inference system for prediction of surface roughness in end milling process using hybrid Taguchi-genetic learning algorithm. *Exp. Syst. Appl.* **36**, 3216–3222 (2009). <https://doi.org/10.1016/j.eswa.2008.01.051>
26. Y.H. Tsai, J.C. Chen, S.J. Lou, An in-process surface recognition system based on neural networks in end milling cutting operations. *Mach. Tools Manuf.* **39**, 583–605 (1999). [https://doi.org/10.1016/S0890-6955\(98\)00053-4](https://doi.org/10.1016/S0890-6955(98)00053-4)
27. P.G. Bernardos, G.C. Vosniakos, Prediction of surface roughness in CNC face milling using Neural Networks and Taguchi's design experiments. *Robot. Comput. Integr. Manuf.* **18**, 343–354 (2002). [https://doi.org/10.1016/S0736-5845\(02\)00005-4](https://doi.org/10.1016/S0736-5845(02)00005-4)
28. A.M. Zain, H. Haron, S. Sharif, Prediction of surface roughness in the end milling machining using Artificial Neural Network. *Exp. Syst. Appl.* **37**, 1755–1768 (2010). <https://doi.org/10.1016/j.eswa.2009.07.033>
29. R.D. Patel, N.V. Oza, S.N. Bhavsar, Prediction of srin CNC milling machine by controlling MPs using, *Int. J. Mech. Eng. Rob. Res.* **3**(4) (2014) ISSN 2278-0149 www.ijmerr.com
30. C.-H. Chen, S.-Y. Jeng, C.-J. Lin, Prediction and analysis of the surface roughness in CNC end milling using neural networks. *Appl. Sci.* **12**, 393 (2022). <https://doi.org/10.3390/app12010393>
31. A.B. Sharkawy, Prediction of surface roughness in end milling process using intelligent systems: a comparative study, Hindawi Publishing Corporation. *Appl. Comput. Intell. Soft Comput.* **2011**, 18 (2011). <https://doi.org/10.1155/2011/183764>
32. A.J. Vallejo, R. Morales-Menendez, R. Ramirez-Mendoza, L. Garza-Castañon, Online prediction of surface roughness in peripheral milling processes, In Proceedings of the European Control Conference 2009, Budapest, Hungary, 2009. <https://doi.org/10.23919/ECC.2009.7074974>
33. A.M.A. Al-Ahmari, Predictive machinability models for a selected hard material in turning operations. *J. Mater. Process. Technol.* **190**, 305–311 (2007). <https://doi.org/10.1016/j.jmatprotec.2007.02.031>
34. J.P. Davim, V.N. Gaitonde, S.R. Karmik, Investigations into the effect of cutting conditions on surface roughness in turning of free machining steel by ANN models. *J. Mater. Process. Technol.* **205**, 16–23 (2008). <https://doi.org/10.1016/j.jmatprotec.2007.11.082>
35. K. Hans, R. Swarup, S. Srivastava, C. Patvardhan, Modeling of manufacturing processes with ANNs for intelligent manufacturing. *Int. J. Mach. Tools Manuf.* **40**, 851–868 (2000). [https://doi.org/10.1016/S0890-6955\(99\)00094-2](https://doi.org/10.1016/S0890-6955(99)00094-2)
36. F. Kafkas, C. Karatas, A. Sozen, E. Arcaklioglu, S. Saritas, Determination of residual stresses based on heat treatment conditions and densities on a hybrid (FLN2-4405) powder metallurgy steel using artificial neural network. *Mater. Des.* **28**, 2431–2442 (2007). <https://doi.org/10.1016/j.matdes.2006.09.003>

37. M. Nalbant, H. Gokkaya, I. Toktas, G. Sur, The experimental investigation of the effects of uncoated, PVD- and CVD-coated cemented carbide inserts and MPs on Surface roughness in CNC turning and its prediction using artificial neural networks. *Robot. Comput.-Integr. Manuf.* **25**, 211–223 (2009). <https://doi.org/10.1016/j.rcim.2007.11.004>
38. J. Sheikh-Ahmad, J. Twomey, ANN constitutive model for high strain-rate deformation of Al 7075–T6. *J. Mater. Process. Technol.* **186**, 339–345 (2007). <https://doi.org/10.1016/j.jmatprotec.2006.11.228>
39. U. Zuperl, F. Cus, Optimization of cutting conditions during cutting by using neural networks. *Robot. Comput.-Integr. Manuf.* **19**, 189–199 (2003). [https://doi.org/10.1016/S0736-5845\(02\)00079-0](https://doi.org/10.1016/S0736-5845(02)00079-0)
40. U. Zuperl, F. Cus, B. Mursec, T. Ploj, A generalized neural network model of ball-end milling force system. *J. Mater. Process. Technol.* **175**, 98–108 (2006). <https://doi.org/10.1016/j.jmatprotec.2005.04.036>
41. M.H.F. A. H., E.Y.T.A. Muataz, HF Al Hazza, E.Y.T. Adesta, M.H.F. Al Hazza, E.Y.T. Adesta, Investigation of the effect of CS on the surface roughness parameters in CNC end milling using artificial neural network, In Proceedings of the IOP Conference Series: Materials Science and Engineering 53(1): 0–12, 2013, <https://doi.org/10.1088/1757-899X/53/1/012089>
42. J. Villarreal, R.N. Lea, R. Savely, Fuzzy logic and neural network technologies. In: 30th Aerospace Sciences Meeting and Exhibit, January 6–9, 1992. <https://doi.org/10.2514/6.1992-868>
43. M. Mohandes, S. Rehman, Estimation of global solar radiation using artificial neural networks. *Renew. Energy* **14**(1–4), 179–184 (1988). [https://doi.org/10.1016/S0960-1481\(98\)00065-2](https://doi.org/10.1016/S0960-1481(98)00065-2)
44. H. Gürbüz, A. Sözen, U. Şeker, Modelling of effects of various chip breaker forms on surface roughness in turning operations by utilizing artificial neural networks. *Politek. Derg.* **19**(1), 71–83 (2016). <https://doi.org/10.2339/2016.19.171-83>
45. J.S.R. Jang, C.T. Sun, *Neuro-Fuzzy and Soft Computing: A Computational Approach to Learning and Machine Intelligence* (Prentice-Hall International, 1997)
46. S.A. Kalogirou, Artificial intelligence for the modeling and control of combustion processes: a review. *Progress in energy and combustion science.* *Prog. Energy Combust. Sci.* **29**, 515–566 (2013). [https://doi.org/10.1016/S0360-1285\(03\)00058-3](https://doi.org/10.1016/S0360-1285(03)00058-3)
47. M.H.F. Al Hazza, E.Y.T. Adesta, Investigation of the effect of CS on the Surface Roughness parameters in CNC end milling using Artificial Neural Network, In Proceedings of the IOP Conference Series: Materials Science and Engineering 53(1), 2013, <https://doi.org/10.1088/1757-899X/53/1/012089>
48. G. Samta, Optimisation of MPs during the face milling of AA5083-H111 with coated and uncoated inserts using Taguchi method. *Int. J. Mach. Mach. Mater.* **17**(3/4), 211–232 (2015). <https://doi.org/10.1504/IJMMM.2015.071993>
49. R.D. Patel, N.V. Oza, S.N. Bhavsar Prediction of surface roughness in CNC milling machine by controlling mps using ANN, *Int. J. Mech. Eng. Rob. Res* **3**(4). 2014, ISSN 2278-0149 www.ijmerr.com
50. J.P. Davim, A note on determination of optimal cutting condition in surface finish obtained in turning using design of experiments. *J. Mater. Process. Technol.* **116**(23), 305–308 (2001)
51. J.P. Davim, L. Figueira, Comparative evaluation of conventional and wiper ceramic tools on cutting forces, surface roughness, and tool wear in hard turning AISI D2 steel. *Proc. Inst. Mech. Eng. Part B: J. Eng. Manuf.* **221**(4), 625–633 (2007). <https://doi.org/10.1243/09544054JEM762>
52. A.A. Ibraheem, S.M. Abdrabbo, H. Gheith, M. Abd El-Salam, M. El-Samanty, Online tool wear monitoring in turning using vibration analysis and artificial neural network. *Ain Shams J. Mech. Eng. (ASJME)* **2**, 201–212 (2009)
53. V.N. Gaitonde, S.R. Karnik, J.P. Davim, Multiperformance optimization in turning of free-machining steel using Taguchi method and utility concept. *J. Mater. Eng. Perform* **18**(3), 231–236 (2009). <https://doi.org/10.1007/s11665-008-9269-6>
54. V.N. Gaitonde, S.R. Karnik, L. Figueira, J.P. Davim, Performance comparison of conventional and wiper ceramic inserts in hard turning through artificial neural network modeling. *Int. J. Adv. Manuf. Technol.* **52**(1), 101–114 (2011)

Publisher's Note Springer Nature remains neutral with regard to jurisdictional claims in published maps and institutional affiliations.

Springer Nature or its licensor (e.g. a society or other partner) holds exclusive rights to this article under a publishing agreement with the author(s) or other rightsholder(s); author self-archiving of the accepted manuscript version of this article is solely governed by the terms of such publishing agreement and applicable law.